https://doi.org/10.5194/egusphere-2026-2381
Preprint. Discussion started: 20 May 2026

BoxMART v1.1 - Box Model for Atmospheric Research and Teaching version 1.1

Putian Zhou[1,2], Zeqi Cui[1,3], Petri Clusius[1,3], Risto Makkonen[2], Zihao Fu[1,3,4], Veli-Matti Kerminen[1], Markku Kulmala[1], and Michael Boy[1,3,5]

[1]Institute for Atmospheric and Earth Systems Research/Physics, University of Helsinki, P.O. Box 64, 00014 Helsinki, Finland
[2]Finnish Meteorological Institute, Erik Palménin aukio 1, 00560, Helsinki, Finland
[3]Atmospheric Modelling Centre Lahti, Lahti University Campus, Lahti, 15140, Finland
[4]State Key Laboratory of Regional Environment and Sustainability, International Joint Laboratory for Regional Pollution Control, Ministry of Education (IJRC), College of Environmental Sciences and Engineering, Peking University, Beijing 100871, China
[5]School of Engineering Sciences, Lappeenranta-Lahti University of Technology LUT, Lahti, 15110, Finland

Correspondence: Putian Zhou (putian.zhou@helsinki.fi)

Abstract. A new open-source chemistry and aerosol box model BoxMART (Box Model for Atmospheric Research and Teaching) has been developed, aiming for easy and flexible configuration for various simulation cases, as well as suitable to teach and learn complex chemistry and aerosol processes. The model is written in Fortran and stored as a gitlab repository. The chemistry module is handled by KPP (Kinetic PreProcessor) which converts the chemistry scheme in an adapted format to Fortran code. The aerosol module currently includes coagulation, condensational and dissolutional growth, evaporation and aerosol thermodynamic processes. The MOSAIC (Model for Simulating Aerosol Interactions and Chemistry) model has been implemented to calculate the non-equilibrium dynamic gas-particle partitioning of non-volatile and semivolatile species, including H_2SO_4, HNO_3, HCl, NH_3, and organic compounds to multiple particle size bins. The current ion system includes H^+, NH_4^+, Na^+, SO_4^{2-}, NO_3^-, Cl^- and H_2O, where pH value in each size bin is also calculated. The particle size distribution is discretized with a fully stationary method. In order to provide good examples for evaluating BoxMART, as well as future model development, a number of benchmark simulation cases from previous studies ranging from simple to complicated cases, have been revised in details and simulated to verify different processes.

1 Introduction

The aerosol particles can affect global radiative forcing by directly scattering or absorbing solar radiation and indirectly altering cloud properties (Forster et al., 2021; Li et al., 2022). The aerosol-cloud interaction (ACI) contributes the largest uncertainty to the present-day global effective radiative forcing estimation due to complex mechanisms (Fig. 7.6 in Forster et al. 2021). For example, aerosol particles can act as cloud condensation nuclei (CCN), indicating that more particles generally produce more cloud droplets, resulting in larger surface area and thus higher cloud albedo when the liquid water content (LWC) is fixed (Twomey, 1977). Additionally, the vertical and horizontal distributions of aerosol particles can affect the liquid water path and cloud fraction (Albrecht, 1989; Gryspeerdt et al., 2019; Pugsley et al., 2025). The aerosol size distribution and composition are

https://doi.org/10.5194/egusphere-2026-2381
Preprint. Discussion started: 20 May 2026

also key factors to determine the aerosol lifetime in the air, number concentration of CCN (Seinfeld and Pandis, 2016), aerosol optical properties (Bond et al., 2013; Saleh et al., 2015; Moise et al., 2015; Riemer et al., 2019) and hygroscopicity (Hodas et al., 2015; Riemer et al., 2019), etc., which influence both direct aerosol radiation effect and ACI. A comprehensive aerosol model is also needed to help us investigate aerosol composition and subsequently reduce the uncertainty of ACI process in large scale models (Sand et al., 2021; Bellouin et al., 2020; Bhatti et al., 2026).

In recent decades, several models have been developed to simulate the aerosol thermodynamic processes, gas-particle partitioning and multiphase chemistry. For example, the Extended Aerosol Inorganics Model (E-AIM) applied the Gibbs free energy minimization algorithm to calculate the thermodynamic equilibrium phase partitioning of inorganic and organic compounds in the atmospheric aerosol particles (Clegg et al., 2001; Wexler and Clegg, 2002; Clegg et al., 2008). It is considered as a benchmark model and widely used to evaluate other aerosol thermodynamic models (Zaveri et al., 2008). However, it is computationally inefficient (Zhang et al., 2000) and can only be used between gas phase and a bulk aerosol phase. Compared to E-AIM, the Equilibrium Solver II (EQUISOLV II) includes additional crustal species cations, e.g., potassium (K^+), calcium (Ca^{2+}) and magnesium (Mg^{2+}), as well as carbonate anion ($CO_3{}^{2-}$). It applies the mass flux iteration and analytical equilibrium iteration methods to solve the equilibrium equations between the gas phase and the aerosol phase with multiple size bins. Moreover, EQUISOLV II can also be used to calculate the non-equilibrium gas-particle transfer when combined with the mass transfer equations (Jacobson, 1999). Another aerosol thermodynamic equilibrium model ISORROPIA II also includes the crustal species like K^+, Ca^{2+} and Mg^{2+}, and computationally efficient (Fountoukis and Nenes, 2007), which makes it suitable for being applied in large scale models, e.g., GEOS-CHEM (Pye et al., 2009). Recently, a simplified but more computationally efficient version ISORROPIA-lite has been developed based on ISORROPIA II, specifically for large scale model applications (Kakavas et al., 2022). However, as E-AIM, ISORROPIA II and ISORROPIA-lite can only calculate equilibrium between bulk aerosol phase and gas phase. In order to solve the non-equilibrium dynamic gas-particle partitioning of non-volatile and semivolatile species between gas phase and particles with multiple size bins, MOSAIC (Model for Simulating Aerosol Interactions and Chemistry) was developed with both accuracy and computational efficiency (Zaveri et al., 2008). It has been also applied in large scale models, e.g., WRF-CHEM (Zhao et al., 2010) and CAM (Zaveri et al., 2021).

Meanwhile, a number of chemistry and aerosol box models with or without aerosol themodynamic processes have also been developed in recent decades, focusing on various research aspects. For example, ARCA box (Atmospherically Relevant Chemistry and Aerosol box model) was developed to simulate complex chemistry and aerosol processes in the atmosphere, smog chamber and flow tube conditions (Clusius et al., 2022) It provides a graphical user interface which facilitates model configuration, simulation monitoring, and preliminary output visualization. However, the aerosol thermodynamic processes are not calculated in ARCA box. PyCHAM (a Python box model for simulating aerosol chambers) also provides a simple GUI, and it is mainly designed for chamber experiments with detailed wall loss processes for gas species and aerosol particles (O'Meara et al., 2021). And similar with ARCA box, PyCHAM does not include a thermodynamic module. Compared to other models, MAFOR v2.0 (Multicomponent Aerosol FORmation model; version 2.0; Karl et al. 2022) and ADCHAM (Aerosol Dynamics, gas- and particle-phase chemistry model for laboratory CHAMber studies; Roldin et al. 2014) have covered more comprehensive processes including aerosol thermodynamics and particle phase chemistry. Both of them are good examples

https://doi.org/10.5194/egusphere-2026-2381
Preprint. Discussion started: 20 May 2026

of incorporating various complex chemistry and aerosol processes in a box model. Inspired by previous models and based on our experiences of model development (Boy et al., 2006, 2011; Zhou et al., 2017a, b), we have developed a new box model BoxMART (Box Model for Atmospheric Research and Teaching) aiming for both research and teaching as said in the full name of the model. Therefore, it is designed to be easy and flexible to set up for various experiments, various chemistry and aerosol processes including aerosol thermodynamics by implementing MOSAIC. Hence, a bunch of benchmark simulation cases from simple to complicated are included in the model and will be described below.

The following sections are organized as below. The model structure and main components are described in Section 2. The benchmark simulation cases are described in details in Section 3. Section 4 includes a summary and discusses the future development plan of the model.

2 Methods

The development of BoxMART is based on SOSAA-Box (model to Simulate Organic vapours, Sulphuric Acid and Aerosols, Box version; Fu et al. 2023). Currently, BoxMART includes a chemistry module and an aerosol module besides general input and output modules (Fig. 1). In the chemistry module, KPP (Kinetic PreProcessor; https://github.com/KineticPreProcessor/KPP; last access on 22.01.2026) is applied to convert the formatted chemistry scheme to Fortran code, which is then called in BoxMART via an interface. The aerosol module calculates the coagulation process following the method originally developed in Jacobson et al. (1994), the condensation, dissolution and evaporation processes following the semi-implicit method originally developed in Jacobson (1997), and the aerosol thermodynamics with MOSAIC (Zaveri et al., 2008). The original code of MOSAIC was downloaded from the official github repository of the WRF-Chem (Weather Research and Forecasting model coupled with Chemistry; Skamarock et al. 2019; https://code.wsl.ch/sharma/CRYOWRF/-/tree/master/WRF, last accessed Apr. 15th, 2026). Then the interface function was modified to fit for BoxMART code. It should be noted that there is a bug in the unit conversion of the Kelvin equation in the original code, which, after communication with Rahul Zaveri, has been fixed in this code. The code is written in Fortran 90, and stored in a GitLab git repository in the University of Helsinki version control server (https://version.helsinki.fi/putian.zhou/boxmart).

2.1 Condensational and dissolutional growth

The condensational and dissolutional growth of particles are calculated following the analytical predictor of condensation (APC) and analytical predictor of dissolution (APD) schemes, respectively, which were originally developed in Jacobson (1997). In order to constrain each species concentration in aerosol phase within a reasonable range, usually larger or equal to 0 and smaller or equal to total species concentration, the constraints described around Eq. 17 in Jacobson (2002) have been also applied. After condensational and dissolutional growth, the particles in each size with new volumes will be redistributed into original stationary size bins. In the redistribution, the number and volume will be conserved except that when new particles are smaller than the smallest size bin or larger than the largest size bin. The calculation is shown below.

https://doi.org/10.5194/egusphere-2026-2381
Preprint. Discussion started: 20 May 2026

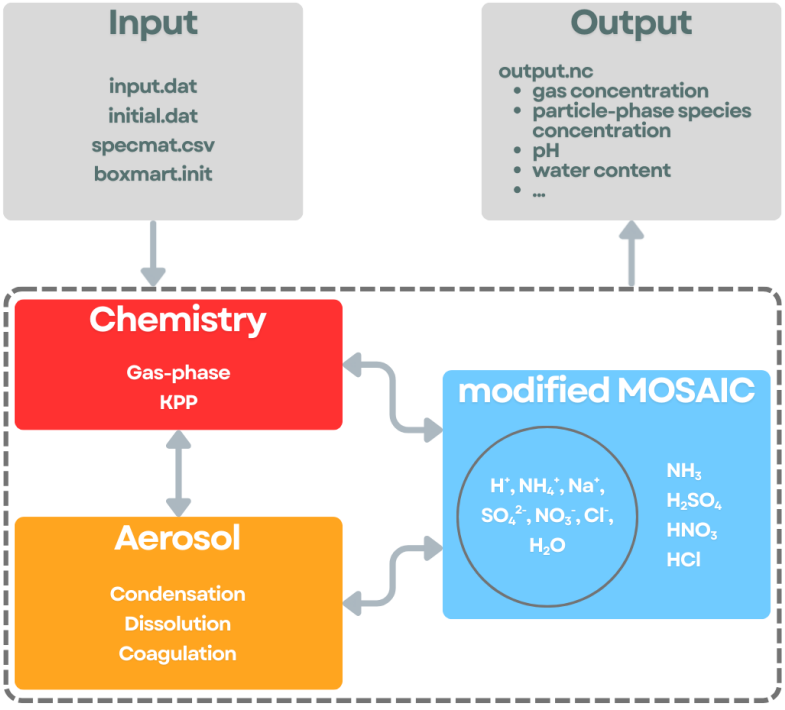

Figure 1. A Model diagram showing the modules included in the model, which are input, output, chemistry, aerosol and MOSAIC modules. The input files for each simulation case are listed in the input box. The output file is a NetCDF (Network Common Data Form) file which stores various output variable data, e.g., number concentrations of gases, number concentrations of particle-phase species in each size bin, pH values and liquid water content in each size bin, etc. Gas-phase chemistry is calculated in the chemistry module, and the chemistry scheme is converted to Fortran code by KPP (Kinetic PreProcessor). The condensational and dissolutional growths, as well as Brownian coagulation are calculated in the aerosol module. The thermodynamic system H^+ - NH_4^+ - Na^+ - SO_4^{2-} - NO_3^- - Cl^- - H_2O along with the gases H_2SO_4, HNO_3, HCl and NH_3, is calculated by MOSAIC (Model for Simulating Aerosol Interactions and Chemistry) module.

Suppose the particles in size bin i grow/shrink from original volume V_i to new volume $V_{i,new}$ which lies between size bin a and $a+1$, the number and volume conservation gives:

$$C_i = C_{a,new} + C_{a+1,new} \tag{1}$$

$$C_i V_{i,new} = C_{a,new} V_a + C_{a+1,new} V_{a+1} \tag{2}$$

https://doi.org/10.5194/egusphere-2026-2381
Preprint. Discussion started: 20 May 2026

here C_i is the particle number concentration in size bin i before growth/shrink, $C_{a,new}$ is the particle number concentration in size bin a contributed by C_i. Solve the equation set, we get:

$$C_{a,new} = C_i r_a \tag{3}$$

$$C_{a+1,new} = C_i(1 - r_a) \tag{4}$$

$$r_a = \frac{V_{a+1} - V_{i,new}}{V_{a+1} - V_a} \tag{5}$$

For particles with $V_{i,new} \leqslant V_1$ or $V_{i,new} \geqslant V_N$, we put all the volume to size bin i or N, respectively. So:

$$C_{1,new} = C_i \frac{V_{i,new}}{V_1}, \text{ when } V_{i,new} \leqslant V_1 \tag{6}$$

$$C_{N,new} = C_i \frac{V_{i,new}}{V_N}, \text{ when } V_{i,new} \geqslant V_N \tag{7}$$

For species in the particle phase, the redistribution follows the volume ratios, so:

$$C_{q,a,new} = C_{q,i,new} r_a \frac{V_a}{V_{i,new}} \tag{8}$$

$$C_{q,a+1,new} = C_{q,i,new}(1 - r_a)\frac{V_{a+1}}{V_{i,new}} \tag{9}$$

$$C_{q,1,new} = C_{q,i,new}, \text{ when } V_{i,new} \leqslant V_1 \tag{10}$$

$$C_{q,N,new} = C_{q,i,new}, \text{ when } V_{i,new} \geqslant V_N \tag{11}$$

where $C_{q,i,new}$ is the number concentration of species q in size bin i after condensation or dissolution, and $C_{q,a,new}$ is the number condensation of species q in size bin a contributed by $C_{q,i,new}$ after growth.

2.2 Coagulation

The Brownian coagulation of particles is calculated based on the semi-implicit method described in Jacobson et al. (1994). This non-iterative method conserves the volume but does not calculate the particle number exactly. However, the error in particle number will decrease when the size bin resolution increases (Jacobson et al., 1994).

Considering the coagulation process, when one particle in size bin i collides with and sticks to another particle in size bin j, an intermediate particle with volume $V_{i,j}$ is formed. Suppose the volume of the intermediate particle lies between size bins k and $k+1$, namely,

$$V_k \leqslant V_{i,j} = V_i + V_j < V_{k+1} \tag{12}$$

then it can be partitioned into size bins k and $k+1$, the volume fraction partitioned to size bin k, namely $f_{i,j,k}$ is calculated from Eq. 13 in Jacobson et al. (1994). The derivation of this equation is shown below.

After coagulation, conserving the particle number and volume we have:

$$\Delta t \beta_{i,j} C_i C_j = \Delta C_k + \Delta C_{k+1} \tag{13}$$

$$\Delta t \beta_{i,j} C_i C_j V_{i,j} = V_k \Delta C_k + V_{k+1} \Delta C_{k+1} \tag{14}$$

https://doi.org/10.5194/egusphere-2026-2381
Preprint. Discussion started: 20 May 2026

where $\beta_{i,j}$ is the coagulation coefficient between a particle from size bin i and a particle from size bin j, the unit of it is $\mathrm{m}^3\ \#^{-1}\ \mathrm{s}^{-1}$). ΔC_k is the change of particle number concentration in size bin k caused by this coagulation process. Δt is the time step. After manipulation of the equation set, we get:

$$\Delta C_{k+1} = \Delta C_k \frac{V_{i,j} - V_k}{V_{k+1} - V_{i,j}} \tag{15}$$

$$\Delta t \beta_{i,j} C_i C_j = \Delta C_k \frac{V_{k+1} - V_k}{V_{k+1} - V_{i,j}} \tag{16}$$

$$V_k \Delta C_k = \Delta t \beta_{i,j} C_i C_j V_k \frac{V_{k+1} - V_{i,j}}{V_{k+1} - V_k} = \Delta t \beta_{i,j} C_i C_j V_{i,j} \frac{V_{k+1} - V_{i,j}}{V_{k+1} - V_k} \frac{V_k}{V_{i,j}} = \Delta t \beta_{i,j} C_i C_j V_{i,j} f_{i,j,k} \tag{17}$$

$$V_{k+1} \Delta C_{k+1} = \Delta t \beta_{i,j} C_i C_j V_{i,j} (1 - f_{i,j,k}) \tag{18}$$

$$\tag{19}$$

Therefore,

$$f_{i,j,k} = \begin{cases} \dfrac{V_{k+1} - V_{i,j}}{V_{k+1} - V_k} \dfrac{V_k}{V_{i,j}} & V_k \leqslant V_{i,j} < V_{k+1} \quad 1 < k < N \\ 1 - \dfrac{V_k - V_{i,j}}{V_k - V_{k-1}} \dfrac{V_{k-1}}{V_{i,j}} & V_{k-1} < V_{i,j} < V_k \\ \dfrac{V_2 - V_{i,j}}{V_2 - V_1} \dfrac{V_1}{V_{i,j}} & V_1 \leqslant V_{i,j} < V_2 \quad k = 1 \\ 1 & V_N \leqslant V_{i,j} \quad k = N \\ 1 - \dfrac{V_N - V_{i,j}}{V_N - V_{N-1}} \dfrac{V_{N-1}}{V_{i,j}} & V_{N-1} < V_{i,j} < V_N \\ 0 & \text{all other cases} \end{cases} \tag{20}$$

where N is the number of size bins.

So the coagulation production term in size bin k (P_k) is calculated as:

$$P_k = \frac{1}{2} \sum_{i=1}^{k} \sum_{j=1}^{k} \Delta t \beta_{i,j} C_i C_j V_{i,j} f_{i,j,k} \tag{21}$$

Here we include coagulation between two particles both in size bin k, since we consider that the intermediate particle volume $2V_k$ could still stay between V_k and V_{k+1} under certain size bin configurations, e.g., $V_{k+1} > 2V_k$. Considering the symmetry of the coagulation,

$$\beta_{i,j} = \beta_{j,i} \tag{22}$$

$$f_{i,j,k} = f_{j,i,k} \tag{23}$$

https://doi.org/10.5194/egusphere-2026-2381
Preprint. Discussion started: 20 May 2026

we can get:

$$
\begin{aligned}
P_k &= \frac{1}{2}\sum_{i=1}^{k}\sum_{j=1}^{k}\beta_{i,j}C_iC_jV_{i,j}f_{i,j,k} \\
&= \frac{1}{2}\sum_{i=1}^{k}\sum_{j=1}^{k}\beta_{i,j}C_iC_j(V_i+V_j)f_{i,j,k} \\
&= \sum_{i=1}^{k}\sum_{j=1}^{k}\beta_{i,j}C_iC_jV_if_{i,j,k}
\end{aligned} \tag{24}
$$

2.3 Aerosol thermodynamic processes

In MOSAIC, the aerosol equilibrium state and water content are computed by the MESA (Multicomponent Equilibrium Solver for Aerosols; Zaveri et al., 2005a) thermodynamics module considering temperature, RH, and the Kelvin effect of different particle size bins. Then the dynamic gas-particle mass transfers of H_2SO_4, HNO_3, HCl and NH_3 are calculated by ASTEM (Adaptive Step Time-split Euler Method; Zaveri et al., 2008). The electrolyte activity coefficients are estimated with Multi-component Taylor Expansion Method (Zaveri et al., 2005b). Then MOSAIC with a modified Kelvin function is implemented into BoxMART with an interface fit to BoxMART main code

3 Results

We have prepared 10 benchmark simulation cases or case sets, which are derived from previous studies. All the cases have been revised since some of them were not described clearly or were illustrated with errors in the original references. In this study, these cases are used to validate the aerosol dynamic processes of coagulation, condensation, and aerosol thermodynamics. A summary of all benchmark simulation cases is given in Table 1.

3.1 Case J1997_APC_TEST

The ideal APC test case in Jacobson (1997) was repeated in this study, and was aimed to ensure that the APC scheme was implemented correctly. The species C1 is assumed to be transferred between gas and particle phases. All the parameters are obtained directly from Jacobson (1997), except the mass transfer rate k_i (0.000833 s^{-1}), which is from Jacobson (2005), where it was fixed from the originally wrong value (0.00833 s^{-1}).

In this simple simulation k_i values are fixed, therefore temperature, air pressure and relative humidity have no effect, whose values can be set to default ones, e.g., 298 K, 1 atm and 80% (these values are applied unless specified in the following cases). In order to be fit for the model simulation with current input files, several other parameters are assumed. The particle size distribution is represented by three bins with their diameters set to 10 nm, 100 nm and 1 μm. The simulation has two components, C1 and CORE, both with particle phase density of 1800 $\mathrm{kg\ m^{-3}}$. C1 exists in both gas and particle phases, whereas CORE only in particle phase. Bins 1 and 2 are initialized with 2 and 5 $\mu\mathrm{g\ m^{-3}}$ of C1 and bin 3 is with 5 $\mu\mathrm{g\ m^{-3}}$ of

https://doi.org/10.5194/egusphere-2026-2381
Preprint. Discussion started: 20 May 2026

Table 1. Summary of benchmark simulation cases. The columns include: case name (Case), sub-case names (Sub-case), aerosol processes verified (Processes), number of size bins (N_b), particle diameter range (D_p in nm), type of initial particle size distribution (Initial), simulation time (t_1), time step (Δt (s)), and references (Reference). "MONO", "LOG", "EXP", and "TRI-LOG" stand for monodisperse, lognormal, exponential, and tri-modal lognormal size distributions, respectively. $\overline{D}_{pg}$ is the geometric mean diameter for lognormal distribution, N_T^0 is the initial total particle number concentration, and GSD is geometric standard deviation. Unless otherwise specified, temperature $T = 298.15$ K, air pressure $P = 1$ atm, RH=80%, the units of diameter and number concentration are nm and $\#\ \mathrm{m}^{-3}$, respectively. A dash (–) indicates not applicable or not specified.

Case	Sub-cases	Processes	N_b	D_p (nm)	Initial distribution	t_1	Δt (s)	Reference
J1997_APC_TEST	–	Condensational growth	3	10, 100, 1000	Preset	4 h	0.1–7200	Jacobson (1997)
J1997_APD_TEST	–	Dissolutional growth	3	10, 100, 1000	Preset	4 h	0.1–7200	Jacobson (1997)
J1994_CASE1	VR12 / VR15 / VR20	Coagulation	39/18/11	6–77/6–60/6–60	MONO: $N_T^0 = 10^{12}$	12 h	600	Jacobson et al. (1994)
J1994_CASE23	GSD14_VR12, GSD115_VR12 / GSD14_VR15, GSD115_VR15 / GSD14_VR20, GSD115_VR20	Coagulation	50/25/15	6–150/6-154/6-152	LOG: GSD = 1.4 or 1.15	6 h	600	Jacobson et al. (1994)
J1994_CASE4	VR15 / VR20	Coagulation	40/24	6–1168/6-1219	EXP: $N_T^0 = 10^{11}$, peak at 100 nm	12 h	600	Jacobson et al. (1994)
J1994_CASE5	–	Coagulation	40	10–82000	TRI-LOG: $\overline{D}_{pg}$ = 13.48, 54.01, 864.1; N_T^0 = $1.038\times10^{11}, 3.228\times10^{10}, 5.381\times10^{6}$; GSD = 1.80, 2.16, 2.21	12 h	600	Jacobson et al. (1994)
JT1995_CASE1	COND, COAG, COND_COAG	Condensation, Coagulation	50	6–150	EXP: $N_T^0 = 10^{11}$, peak at 20 nm	6 h	600	Jacobson and Turco (1995)
JT1995_CASE2	KELVIN, NO_KELVIN	Condensation, Coagulation, Kelvin effect	80	6–931	LOG: $\overline{D}_{pg}$ = 20, GSD = 1.4, $N_T^0 = 10^{12}$	30 min	10	Jacobson and Turco (1995)
JT1995_CASE3	F4_COND / F5_COND, F5_COAG, F5_COND_COAG / F6_COND, F6_COAG, F6_COND_COAG	Condensation, Coagulation	42/45/36	10–2550/40–740/100–11334	LOG: F4 ($\overline{D}_{pg}$ = 200, GSD = 1.4, $N_T^0 = 2.26\times10^{13}$); F5 ($\overline{D}_{pg}$ = 100, GSD = 1.1447, $N_T^0 = 8.796\times10^{12}$); F6 ($\overline{D}_{pg}$ = 600, GSD = 1.3084, $N_T^0 = 6.387\times10^{12}$)	10000/5/10000 s	1000/0.01/100	Jacobson and Turco (1995)
Z2008_CASE1–12	CASE1, 2, 4, 5, 6, 7, 8, 9, 11, 12	Aerosol thermodynamics [a]	1	300–1000 [b]	MONO: $N_T^0 = 5.08\times10^{6}$–1.462×10^{9} [c]	1.5 h – 15 h [d]	10–100 [e]	Zaveri et al. (2008)
Z2008_CASE13	–	Thermodynamics, condensation, coagulation; RH=30%	100	5–12000	TRI-LOG: $\overline{D}_{pg}$ = 10, 100, 2000 nm; N_T^0 = $5\times10^{10}, 1.2\times10^{9}, 6\times10^{5}$; GSD = 1.5, 1.7, 1.8	10 h	60	Zaveri et al. (2008)
Z2008_CASE14	OLD (original Kelvin), NEW (corrected Kelvin)	Thermodynamics, condensation, coagulation; RH=85%	100	5–12000	TRI-LOG: $\overline{D}_{pg}$ = 10, 100, 2000 nm; N_T^0 = $5\times10^{10}, 1.2\times10^{9}, 6\times10^{5}$; GSD = 1.5, 1.7, 1.8	10 h	60	Zaveri et al. (2008)

[a] RH is 30% in CASE1 and 2, 85% in CASE4, 5, 6 and 7, 55% in CASE8, 52% in CASE9, respectively. RH varies from 30% to 70% in CASE11, and from 70% to 30% in CASE12.

[b] The monodisperse diameter is 300 in CASE1, 4 and 5, 1000 in CASE2 and 9, 800 in CASE6 and 7, 500 in CASE8 and 12, respectively.

[c] The initial total particle number concentration is 1.462×10^{9} in CASE1, 5.08×10^{6} in CASE2 and 11, 1.46×10^{7} in CASE3, 4.23×10^{7} in CASE4 and 5, 9.9×10^{6} in CASE6, 1.16×10^{7} in CASE7, 1.024×10^{8} in CASE8 and 12, 1.02×10^{7} in CASE9, respectively.

[d] The simulation time is 4 h in CASE1, 4 and 9, 6 h in CASE2, 5 h in CASE5, 6 and 7, 1.5 h in CASE8, 15 h in CASE11 and 12, respectively.

[e] The time step is 100 s in CASE1, 2, 4, 5, 6, 7, 8 and 9, 10 s in CASE11 and 12, respectively.

https://doi.org/10.5194/egusphere-2026-2381
Preprint. Discussion started: 20 May 2026

Table 2. Parameters and results in the case J1997_APC_TEST. The columns include: particle bins in which the gas phase is also listed (Bin), particle diameter (D_p (nm)), initial particle number concentration (N (# m^{-3})), mass transfer rate (k (s^{-1})), initial mass concentration (Initial (μg m^{-3})) of species C1 and CORE, simulation results of C1 after four hours (Results (μg m^{-3})) in the model and reference.

Bin	D_p (nm)	N (# m^{-3})	k (s^{-1})	Initial (μg m^{-3})		Results (μg m^{-3})	
				C1	CORE	Model	Reference
1	10	2.1221×10^{12}	0.000833	2.0	0.0	2.182	2.18
2	100	5.3052×10^{9}	0.001667	5.0	0.0	5.364	5.36
3	1000	5.3052×10^{6}	0.00667	0.0	5.0	1.455	1.46
Gas				3.0		1.000	1.00

CORE. The initial number concentration in size bin i can be calculated as:

$$N_i = M_i/(V_i * \rho_{p,i}) \tag{25}$$

where N_i (# m^{-3}) is the particle number concentration, M_i (kg m^{-3}) is the particle mass concentration. V_i (m^3) is the single particle volume, ρ_p is the particle density. All the parameters and results are listed in Table 2. The results after 4-h simulation are independent on the selected model timestep (0.1 – 7200 s), and agree with the results in Jacobson (1997).

3.2 Case J1997_APD_TEST

This case was aimed to ensure that the APD scheme was implemented correctly. The setup is similar with the case J1997_APC_TEST, except that the Henry's law constant (i.e. Henry solubility H_{cp}, see the detailed definitions and name conventions in Sander (2015)) of C1 in size bin i should be explicitly calculated according to:

$$H_i' = LWC_i R_{atm} T H_{cp} \tag{26}$$

where H_i' is dimensionless Henry's law constant, which is set to 4.0 in this case according to Jacobson (1997). The liquid water content (LWC) in each size bin is assumed to be 1.0 μg m^{-3}. The gas constant R_{atm} is 8.206 m^3 atm K^{-1} mol^{-1}, and T is 298 K. So H_{cp} is 1.6358×10^{11} M atm^{-1}. The results after 4-h simulation are independent on the selected model timestep (0.1 – 7200 s), and agree with the results in Jacobson (1997).

3.3 Case J1994_CASE1

In this case the simulation is compared to an analytical case originally described in von Smoluchowski (1918). This case is aimed to ensure that the coagulation scheme is implemented correctly, so the condensation is not calculated. The initial particle size distribution is monodisperse and all particles only contain one component, assuming as CORE_aq. The coagulation kernel

https://doi.org/10.5194/egusphere-2026-2381
Preprint. Discussion started: 20 May 2026

Table 3. The same as Table 2 excpet for the case J1997_APD_TEST

Bin	Dp (nm)	N (# m^{-3})	k (s^{-1})	Initial ($\mu g\ m^{-3}$)		Results ($\mu g\ m^{-3}$)	
				C1	CORE	Model	Reference
1	10	1.0610×10^{12}	0.00333	0.0	1.0	3.077	3.08
2	100	1.0610×10^{9}	0.00833	0.0	1.0	3.077	3.08
3	1000	1.0610×10^{6}	0.0117	0.0	1.0	3.077	3.08
Gas				10.0		0.769	0.769

is assumed to be a constant as:

$$\beta = \frac{8k_BT}{3\eta} \tag{27}$$

where k_B is Boltzmann constant (1.38×10^{-23} J K^{-1}), η is the dynamic viscosity of air (kg m^{-1} s^{-1}). Here we assume T as 298.15 K, and then $\eta = 1.85 \times 10^{-5}$ kg m^{-1} s^{-1}, so $\beta = 5.93 \times 10^{-16}$ m^3 $\#^{-1}$ s^{-1}. The analytical solution of the particle number size distribution for bin i at time t (N_i^t) can be calculated as:

$$N_i^t = \frac{N_1^0(0.5\beta N_1^0 t)^{i-1}}{(1+0.5\beta N_1^0 t)^{i+1}} \tag{28}$$

where N_1^0 is the initial number concentration in the first bin, and t is the time which should be larger than 0. Following the simulation case in Jacobson et al. (1994), N_1^0 is set to 10^{12} # m^{-3}, and three size bin configurations are simulated with different volume ratios (V_r) of 1.2 (39 bins, labelled with VR12), 1.5 (18 bins, labelled with VR15), and 2.0 (11 bins, labelled with VR20). These labels have the same meanings in the following cases. The bin structure is constructed with method 8 (Appendix A) for J1994_CASE1_VR12.

Figure 2 shows the analytical solution and the simulation results after 12 hours with time step of 600 seconds. The model results agree the best with the analytical solution for the sub-case J1994_CASE1_VR12 and deviate more when the size bin resolution decreases, as expected. It should be noted that the size distribution for particles smaller than 10 nm shows more discontinuity in J1994_CASE1_VR12 and J1994_CASE1_VR15 than J1994_CASE1_VR20, which results from the coagulation dips as explained in Appendix A.

3.4 Case J1994_CASE23

In this case the simulations results are compared to the cases 2 and 3 in Jacobson et al. (1994). The parameters and configurations are similar with the case J1994_CASE1 except the initial conditions. Here the initial particle number size distribution follows the lognormal distribution with geometric standard deviation (GSD) of 1.4 (in sub-cases J1994_CASE23_GSD14_VR12, J1994_CASE23_GSD14_VR15, J1994_CASE23_GSD14_VR20) and 1.15 (in sub-cases J1994_CASE23_GSD115_VR12, J1994_CASE23_GSD115_VR15, J1994_CASE23_GSD115_VR20) , respectively. In order to cover the whole range of the

https://doi.org/10.5194/egusphere-2026-2381
Preprint. Discussion started: 20 May 2026

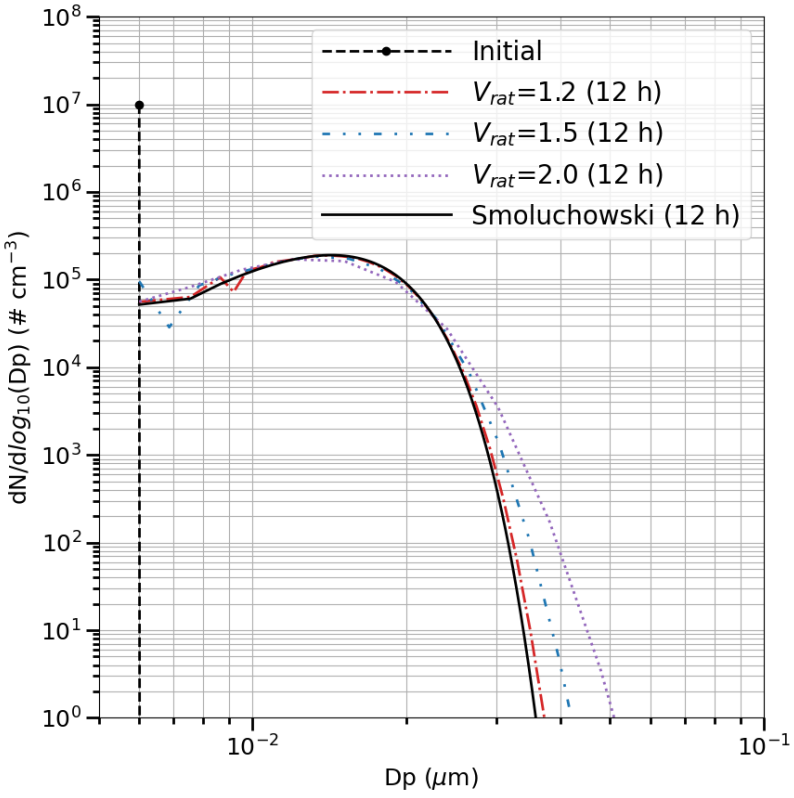

Figure 2. Simulation results of particle number size distribution after 12 hours of sub-cases J1994_CASE1_VR12 (red), J1994_CASE1_VR15 (blue) and J1994_CASE1_VR20 (purple) in the case of J1994_CASE1. The initial value (black point with dashed line) and analytical solution (black solid line) are also shown.

results shown in Jacobson et al. (1994), the number of size bins are set to 50, 25, 15 for VR12, VR15, VR20 sub-cases, respectively. The largest size bin diameters (geometric mean diameter, GMD) in these sub-cases are around 150 nm. The simulation time is 6 hours with time step of 600 seconds.

The simulation results agree well with that in Jacobson et al. (1994), which show a diffusion to larger particles as time progresses (Fig. 3). The simulations with higher volume ratios show similar results with slightly more diffusion to larger particles (Figs. 3b, c, e and f).

3.5 Case J1994_CASE4

This simulation case including two sub-cases J1994_CASE4_VR15 and J1994_CASE4_VR20 is compared to the case 4 in Jacobson et al. (1994). Again, the parameters and configurations are similar with Case J1994_CASE1 except the initial conditions, which is an exponentially spread size distribution described in Eq. 25 in Jacobson et al. (1994) with $\Delta t = 0$. Here the initial total number concentration is set to 10^{11} # m^{-3}, and the size bin with the peak number concentration is 100 nm.

https://doi.org/10.5194/egusphere-2026-2381
Preprint. Discussion started: 20 May 2026

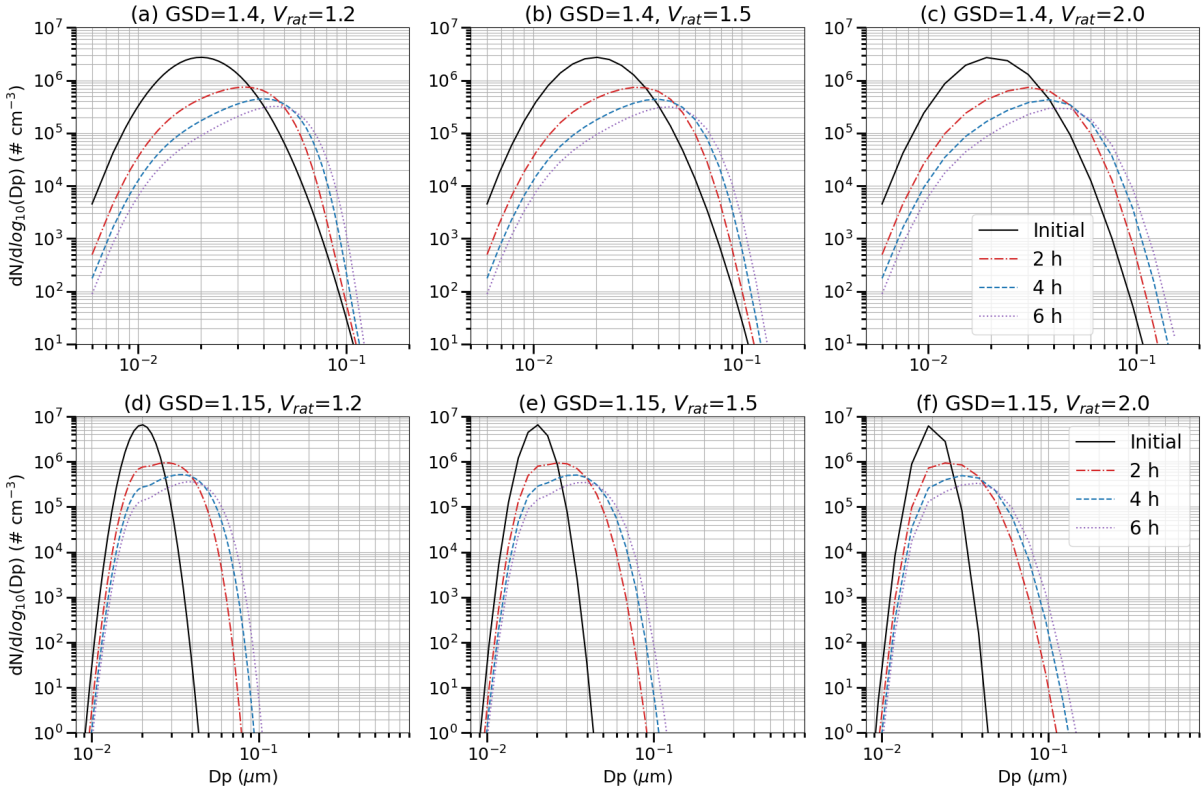

Figure 3. Simulated particle number size distributions (PNSD) at initial time (black solid line), after 2 hours (red dot dashed line), after 4 hours (blue dashed line), and after 6 hours (purple dotted line) are shown for sub-cases in the case J1994_CASE23. The sub-cases with geometric standard deviation (GSD) of 1.4 are shown in the upper panel, which have applied volume ratios of (a) 1.2, (b) 1.5 and (c) 2.0, respectively. The ones with GSD of 1.15 are shown in the lower panel with volume ratios of (d) 1.2, (e) 1.5 and (f) 2.0, respectively.

The size bin starts from 6 nm with 40 bins in J1994_CASE4_VR15 and 24 bins in J1994_CASE4_VR20. The simulation time is 12 hours. Figure 4 shows that our results of both sub-cases shift slightly more to the larger size bins than the results in Jacobson et al. (1994), indicating slightly larger numerical diffusion in the large size bins.

3.6 Case J1994_CASE5

In this case a continuous tri-modal size distribution was simulated. The parameters given in Jacobson et al. (1994) were for volume distribution, so we need to convert them to number size distribution. According to the Eq. 8.52 in Chap. 8.1 in Seinfeld and Pandis (2016), the geometric standard deviations (σ_g) are the same for these two moments, which is 1.8, 2.16 and 2.21 for three modes, respectively. The relation between volume median diameter ($\overline{D}_{pgV}$) and median diameter ($\overline{D}_{pg}$) is:

$$\ln \overline{D}_{pgV} = \ln \overline{D}_{pg} + 3 \ln^2 \sigma_g \tag{29}$$

https://doi.org/10.5194/egusphere-2026-2381
Preprint. Discussion started: 20 May 2026

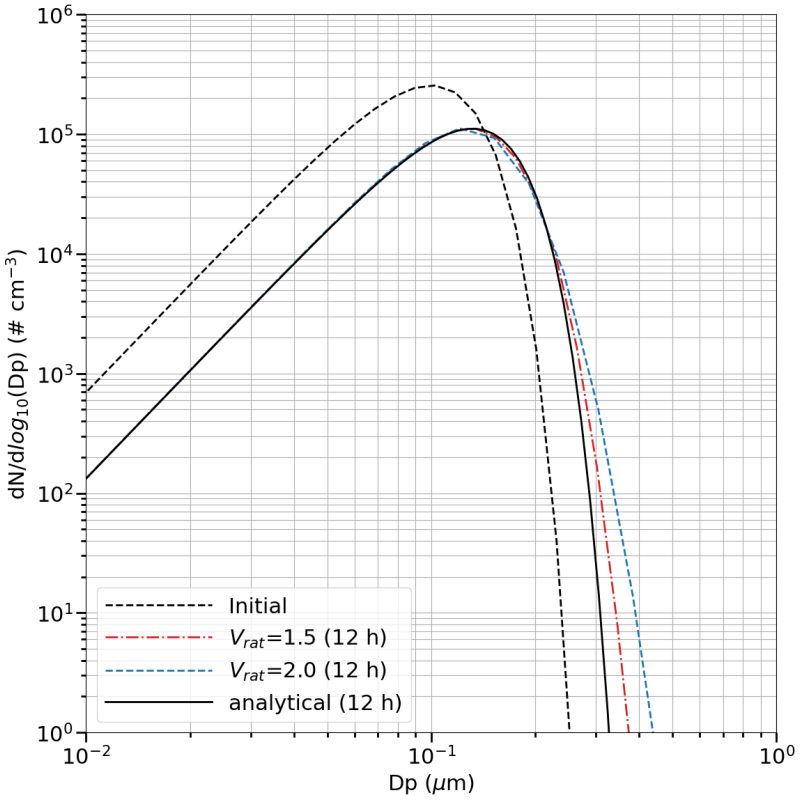

Figure 4. Simulated particle number size distributions (PNSD) at initial time (black dashed line) and after 12 hours are shown for sub-cases J1994_CASE4_VR15 (red dot dashed line) with volume ratio 1.5 and J1994_CASE4_VR20 (blue dashed line) with volume ratio 2.0. The analytical solution after 12 hours is also shown (black solid line).

And the total volume concentration (V_t) can be calculated as:

$$V_t = \frac{\pi}{6} N_t \exp(3 \ln \overline{D}_{pg} + \frac{9}{2} \ln^2 \sigma_g) \tag{30}$$

So $\overline{D}_{pg}$ is 13.48 nm, 54.01 nm and 864.1 nm, the number concentration N_t is 1.038×10^{11} # m^{-3}, 3.228×10^{10} # m^{-3} and 5.381×10^{6} # m^{-3}, for three modes, respectively. The volume ratio between adjacent bins is 2, and number of bins is 40 with the first bin diameter as 10 nm. The Brownian coagulation kernel is applied to calculate the coagulation process.

The simulation results show good agreement with the results in Jacobson et al. (1994) (Fig. 5a). Zhang et al. (1999) simulated the same case, which is the urban condition case in that study. The number size distribution shown here (Fig. 5b) also agrees well with the exact results in Zhang et al. (1999) above 10 nm, which is the smallest size bin diameter in our case.

https://doi.org/10.5194/egusphere-2026-2381
Preprint. Discussion started: 20 May 2026

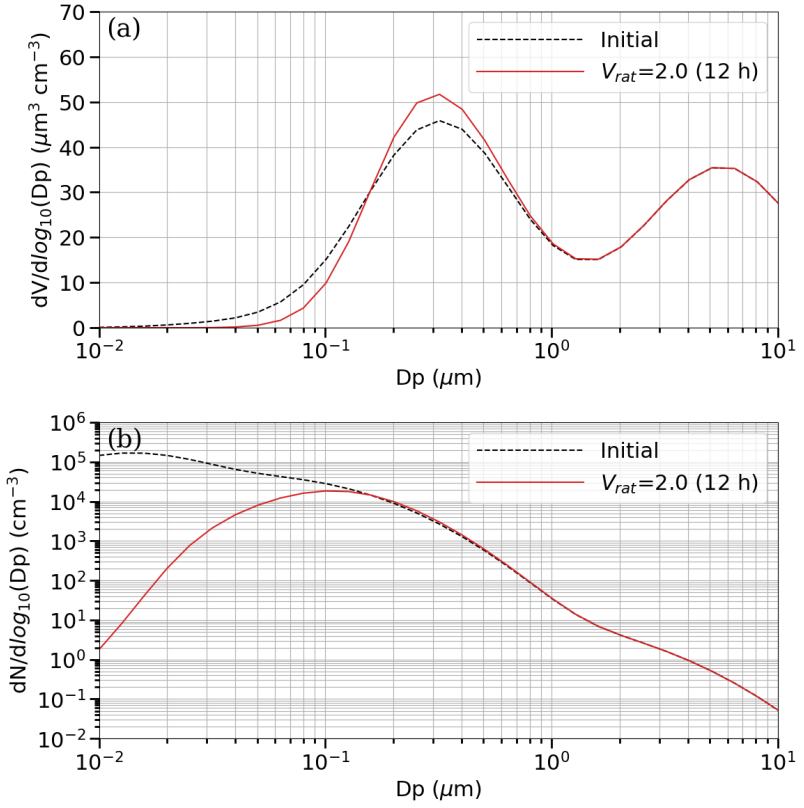

Figure 5. (a) Simulated particle volume size distributions at initial time (black dashed line) and after 12 hours (red solid lines) and (b) Simulated particle number size distributions at initial time (black dashed line) and after 12 hours (red solid lines) in the case J1994_CASE5. The volume ratio between adjacent size bins is 2.0.

3.7 Case JT1995_CASE1

In this case, the evolution of a self-perserving distribution with condensational growth and coagulation was simulated, referring to the first case in Jacobson and Turco (1995). The initial number concentration size distribution at bin k is

$$N_k^0 = \frac{N_T^0 \mathrm{d}V_k}{V_p} \exp\left(-\frac{V_k}{V_p}\right) \tag{31}$$

where N_T^0 is the initial total number concentration, V_k is the particle volume at bin k, $\mathrm{d}V_k$ is the volume range of size bin k, and V_p is the initial mean volume of all particles, which is 20 nm in this simulation. With fixed condensational growth rate and fixed coagulation kernel, the analytical solution at time t is given by Gelbard and Seinfeld (1978) as:

$$N_k^t = \frac{4N_T^0 \mathrm{d}V_k}{V_p(\tau+2)^2} \exp\left(-\frac{2V_k}{V_p(\tau+2)} \exp(-\sigma t) - \sigma t\right) \tag{32}$$

https://doi.org/10.5194/egusphere-2026-2381
Preprint. Discussion started: 20 May 2026

where

$$\tau = N_T^0 \beta t \tag{33}$$

$$\beta = \frac{8 k_B T}{3\eta} \tag{34}$$

$$\sigma = N_T^0 \beta \tag{35}$$

the parameters are the same as that in J1994_CASE1 (Table 1). σ is the growth rate (s^{-1}). In this case, $N_T^0 = 10^{11}$ # m^{-3}, the volume ratio between adjacent bins $V_r = 1.2$, and the number of bins is 50. As in Jacobson and Turco (1995), $\beta = 0$ when only growth is considered, and $\sigma = 0$ when only coagulation is considered. Three sub-cases COND (only growth), COAG (only coagulation), and COND_COAG (with both growth and coagulation) were simulated and compared with the results in Jacobson and Turco (1995).

For distributing the particles, a hybrid method in Jacobson and Turco (1995) was applied, in which the particles are distributed into different size bins according to their involatile core diameter. The condensed/evaporated species only increase/decrease the particle volume in a size bin, but they are still in the same size bin as long as the core size is not changed. The concept of how condensable species are treated is similar with how water in a particle is treated in our model, hence the growth rate is calculated as the water growth in this simulation. According to Eq. 11 in Jacobson and Turco (1995), the actual growth after each time step Δt at bin k is calculated as:

$$V_{k,wet}^{t+\Delta t} = V_{k,wet}^{t} + \sigma V_{k,wet}^{t} \Delta t \tag{36}$$

here $V_{k,wet}$ is the particle wet volume at bin k. Figure 6 shows that our simulation results agree well with the analytical solutions in all three sub-cases. Notice that here the x axis is the particle wet diameter ($D_{p,wet}$) instead of dry diameter.

3.8 Case JT1995_CASE2

This case refers to the second case in Jacobson and Turco (1995), which includes an involatile species V_1 and a condensable species V_2. the saturation vapor pressure of V_2 is 7.5×10^{-7} Pa, corresponding to parameters $A = -11.1307$ and $B = 0$ with the equation used in our model:

$$P_s = P_{\text{atm}} * 10^{A - \frac{B}{T}} \tag{37}$$

where P_s is the saturation vapor pressure with unit of Pa, P_{atm} is standard atmosphere pressure equal to 1.01325×10^5 Pa, A and B are parameters, and T is air temperature with the value of 298.15 K here. The molar masses of them are 0.15 kg mol^{-1}, and the densities of them in the particle phase are 1500 kg m^{-3}. The effective diffusion coefficient of gaseous V_2 ($D_{V_2}^{\text{eff}}$) is 10^{-5} m^2 s^{-1}, which is applied in the calculation of mass transfer coefficient k_m of species q at bin k:

$$k_m = N_k 2\pi D_{p,k} D_q^{\text{eff}} \tag{38}$$

The surface tension of both species in the particle phase is 0.03 N m^{-1}. A Brownian coagulation kernel is applied.

https://doi.org/10.5194/egusphere-2026-2381
Preprint. Discussion started: 20 May 2026

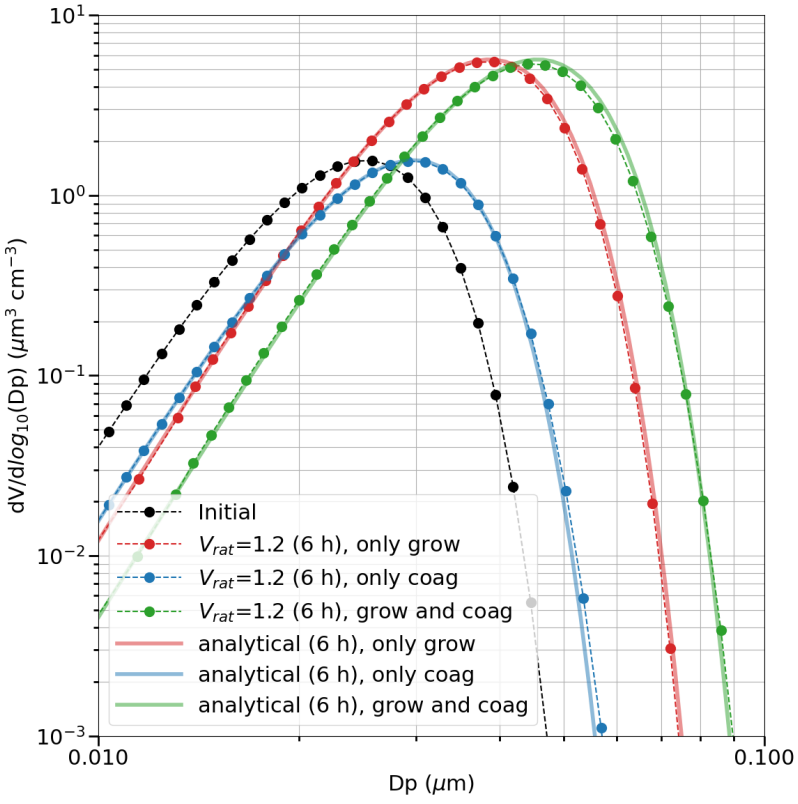

Figure 6. Simulated particle volume size distributions (dashed lines with circle markers) at initial time (black), after 6 hours with only condensational growth in JT1995_CASE1_COND (red), after 6 hours with only coagulation in JT1995_CASE1_COAG (blue), and after 6 hours with both condensational growth and coagulation in JT1995_CASE1_COND_COAG (green). The analytical solutions corresponding to the sub-cases are also plotted (solid lines). The volume ratio between adjacent size bins is 1.2. D_p is the particle wet diameter $D_{p,wet}$.

In the beginning, the particle is distributed as a lognormal distribution mode with the geometric mean number diameter of 20 nm, geometric standard deviation of 1.4, and total particle number concentration of 10^{12} # m^{-3}. Each particle volume contains half V_1 and half V_2. The gas partial pressure of V_2 is 1.3×10^{-5} Pa, corresponding to a number concentration of 3.1582×10^{15} # m^{-3}. The simulation time is 30 minutes.

Two sub-cases were simulated, one with Kelvin effect (KELVIN) and the other without (NO_KELVIN). Here we applied 80 size bins with volume ratio as 1.2, and the particle diameters range from 6 nm to about 931 nm. Figure 7 shows that our simulation results agree generally well with that in Jacobson and Turco (1995) in both sub-cases. V_2 condensed evenly onto particles with different sizes in the case NO_KELVIN, while in the case KELVIN V_2 nearly only exists in particles larger than 20 nm after 30 minutes because of the transfer from small particles to large particles under Kelvin effect. While the amount of V_1 in each size bin is only affected by coagulation, in the case KELVIN small particles almost only contain V_1, and large particles contain less V_1 than V_2 due to condensation of V_2.

https://doi.org/10.5194/egusphere-2026-2381
Preprint. Discussion started: 20 May 2026

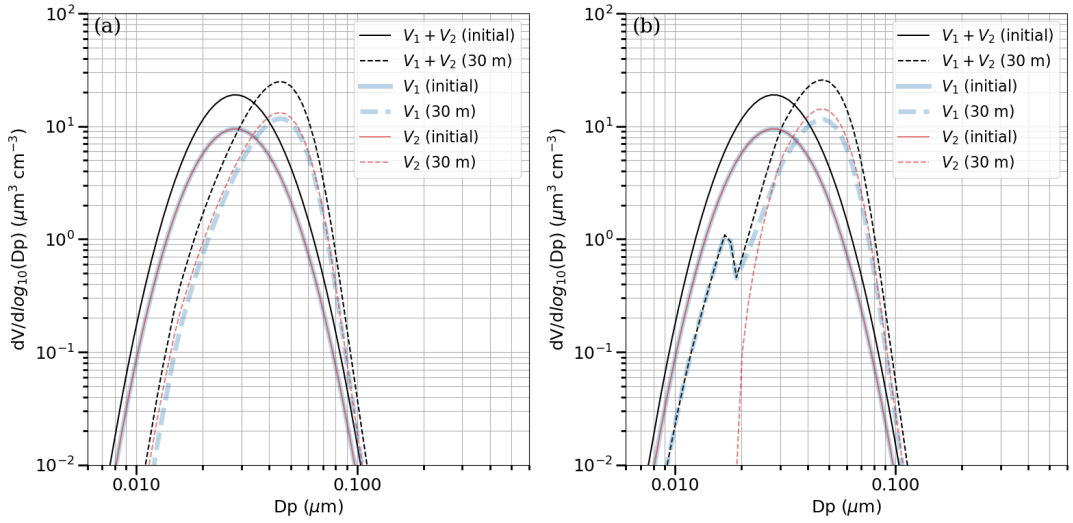

Figure 7. Simulated particle volume size distributions (PVSD) (a) without and (b) with Kelvin effect in the cases JT1995_CASE2_KELVIN and JT1995_CASE2_NO_KELVIN, respectively. The PVSD of $V_1 + V_2$ (black), V_1 (blue) and V_2 (red) at the initial time (solid line) and after 30 minutes (dashed line) are plotted, respectively.

However, some differences still exist. In our simulations, the stationary method assumes that particles grow/shrink and are then redistributed into larger/smaller bins without altering the size within a bin. While in a hybrid method applied in Jacobson and Turco (1995), the particles in small size bins can grow and stay within their size bins if the involatile cores do not change. Consequently, the stationary method results in a numerical diffusion of size bins, distributing some partilces in smaller size bins and larger size bins. With coagulation, this will finally cause a faster elimination of small particles and an increased growth of large particles compared to the hybrid method. That could explain why our results show a shift to larger size bins compared to that in Jacobson and Turco (1995).

3.9 Case JT1995_CASE3

In this case, which refers to the third set of cases in Jacobson and Turco (1995), the condensational growth is simulated and compared with the analytical solutions in the sub-cases F4_COND, F5_COND and F6_COND. The lognormal PNSDs with different parameters are applied as the initial conditions (Table 4). In cases labelled with COAG, only coagulation is simulated, and with COND_COAG, both condensational growth and coagulation are simulated. The initial conditions, model configuration parameters, model results and analytical solutions are listed in Table 4, similar as Table 1 in Jacobson and Turco (1995).

https://doi.org/10.5194/egusphere-2026-2381
Preprint. Discussion started: 20 May 2026

Table 4. The initial conditions, model configuration parameters, the model results and analytical solutions of final total volume concentrations are listed. Here only the sub-cases F4_COND, F5_COND and F6_COND are listed because analytical solutions are available for them. $D_{pg,0}$ is the geometric mean diameter of the initial lognormal distribution, $\sigma_{g,0}$ is the geometric standard deviation of the initial distribution, $N_{T,0}$ is the initial total particle number concentration, $V_{T,0}$ is the initial total particle volume concentration, $V_{Ta,1}$ is the analytical solution of final total volume concentration, $V_{Tm,1}$ is the simulated final total volume concentration, V_r is the volume ratio of adjacent size bins, A_D is the growth parameter, Δt is the model time step, t_1 is the simulation time in a model run.

	$D_{pg,0}$	$\sigma_{g,0}$	$N_{T,0}$	$V_{T,0}$	$V_{Ta,1}$	$V_{Tm,1}$	V_r	A_D	Δt	t_1
	μm	-	# cm^{-3}	μm^3 cm^{-3}	μm^3 cm^{-3}	μm^3 cm^{-3}	-	m^2 s^{-1}	s	s
F4_COND	0.2	1.4000	2.260×10^7	1.576×10^5	2.467×10^5	2.449×10^5	1.5	1.06×10^{-18}	1000	10000
F5_COND	0.1	1.1447	8.796×10^6	5.000×10^3	1.689×10^5	1.656×10^5	1.2	1.00×10^{-14}	0.01	5
F6_COND	0.6	1.3084	6.387×10^6	9.999×10^5	1.703×10^6	1.693×10^6	1.5	1.00×10^{-17}	100	10000

The analytical solution of number concentration at each size bin i at time t_1 with a constant growth term A_D is shown as below:

$$N_{i,a}(t_1) = \frac{N_{T,0}}{\sqrt{2\pi}\ln(10)\log_{10}\sigma_g} \frac{D_{p,i}\Delta D_{p,i}}{D_{p,i}^2 - 2A_D t_1} \exp\left[\frac{\log_{10}^2\left(\sqrt{D_{p,i}^2 - 2A_D t_1}/D_{pg,0}\right)}{2\log_{10}^2\sigma_g}\right] \tag{39}$$

where the constant $\ln(10)$ is used to convert base-10 logarism to natural logarism, $\Delta D_{p,i}$ is the width of the size bin i. A_D is the term applied to calulcate the growth of particle diameter as below:

$$\frac{\mathrm{d}D_p}{\mathrm{d}t} = \frac{A_D}{D_p} \tag{40}$$

So the volume growth rate is calculated as:

$$\frac{\mathrm{d}V}{\mathrm{d}t} = \frac{\mathrm{d}}{\mathrm{d}t}\left(\frac{1}{6}\pi D_p^3\right) = \frac{\pi}{2} D_p A_D \tag{41}$$

The results of case F4_COND are shown in Fig. 8a, and it should be noticed that the data in y-axis are the volume size distribution with unit μm^3 cm^{-3} instead of the number concentration size distribution, which could be a typo in Fig. 4 in Jacobson and Turco (1995). Our model results show much more particles in the lower end compared to analytical solution due to numerical diffusion of the stationary method. However, the modelled final total particle volume ($V_{Tm,1}$) agrees well with the analytical solution ($V_{Ta,1}$) and the model results in Jacobson and Turco (1995). The slightly lower value of $V_{Tm,1}$ compared to $V_{Ta,1}$ can be explained by the overestimate of smaller particles, since the growth is proportional to particle diameter (Eq. 41).

Our results of case F5_COND shown in Fig. 8b are quite different from that in Fig. 5 in Jacobson and Turco (1995). First, the analytical solution in our case F5_COND grows larger with higher peak number size distribution of 7×10^8 # cm^{-3}. The total volume concentration of analytical solution in our simulation at the end (5 s) is 1.689×10^5 μm^3 cm^{-3}, which is also much larger than that in Jacobson and Turco (1995) (7.06×10^4 μm^3 cm^{-3}). The final total volume concentration in our model result is similar with our analytical solution, although it still shows large numerical diffusion. The results with coagulation in

https://doi.org/10.5194/egusphere-2026-2381
Preprint. Discussion started: 20 May 2026

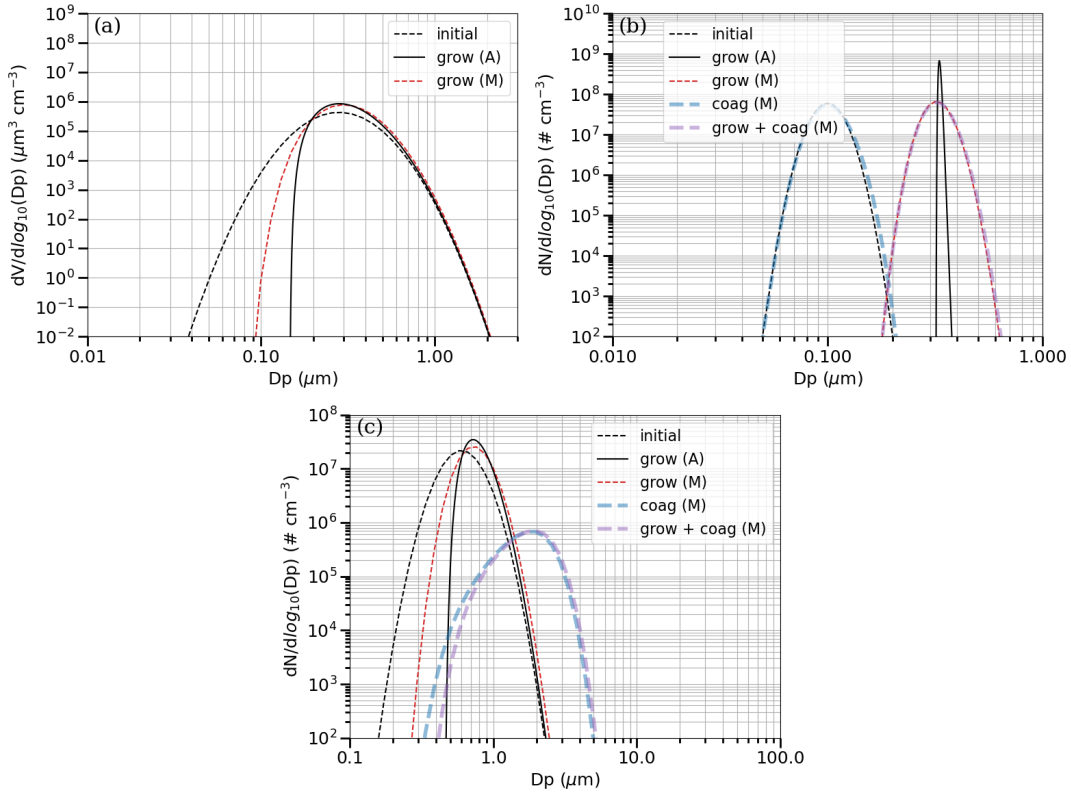

Figure 8. The comparisons between the model results and analytical solutions of particle number size distributions in sub-cases (a) F4_COND (red dashed line), (b) F5_COND (red dashed line), F5_COAG (blue dashed line), F5_COND_COAG (purple dashed line) (c) F6_COND (red dashed line), F6_COAG (blue dashed line), F6_COND_COAG (purple dashed line). The simulation time is 10000 seconds, 5 seconds and 10000 seconds in F4_COND, F5 cases and F6 cases, respectively. The analytical solutions (solid black line) are only available for the sub-cases F4_COND, F5_COND and F6_COND. The initial conditions (black dashed line) are also shown for each sub-case set (F4, F5 and F6).

our simulations F5_COAG and F5_COND_COAG show little shift of the aerosol size distribution, which is consistent with the very short simulation time 5 s. However, the results in Jacobson and Turco (1995) show apparent shift due to coagulation which seems not reasonable, unless the coagulation kernel is very strong.

In case F6_COND, our model results still show numerical diffusion compared to the analytical solution (Fig. 8c). Similarly, the final total volume concentration in our simulations is apparently higher than that in Jacobson and Turco (1995). Moreover, the coagulation does not shift the size distribution as large as that in Jacobson and Turco (1995).

In summary, the results with the stationary method agree with the analytical solution in average. but it will introduce numerical diffusion which is even larger when the growth process is dominant. And it should be noted that our results are different from that in Jacobson and Turco (1995) in sub-cases F5_COND, F5_COAG, F5_COND_COAG, F6_COND, F6_COAG and F6_COND_COAG, which indicates further verification of these cases is still needed.

https://doi.org/10.5194/egusphere-2026-2381
Preprint. Discussion started: 20 May 2026

3.10 Case Z2008_CASE

In order to verify the performance of how the aerosol thermodynamic processes are calculated in BoxMART, the test cases in Zaveri et al. (2008) were simulated in this study. Since the calcium ion (Ca^{2+}) is not included in the current model version, only the cases 1, 2, 4, 5, 6, 7, 8, 9, 11, 12, 13, and 14 in Zaveri et al. (2008) were simulated, which corresponded to sub-cases Z2008_CASE1, Z2008_CASE2, Z2008_CASE4, Z2008_CASE5, Z2008_CASE6, Z2008_CASE7, Z2008_CASE8, Z2008_CASE9, Z2008_CASE11, Z2008_CASE12, Z2008_CASE13, and Z2008_CASE14 in this study. The cases from Z2008_CASE1 to Z2008_CASE12 are discussed in Appendix B, since they are mostly applied to evaluate how MOSAIC is performing in BoxMART as a single module. In the Z2008_CASE set simulations, the ion HSO_4^- is not explicitly output and calculated from MOSAIC, so the sulfate actually represents SO_4^{2-} + HSO_4^-. In the beginning of each simulation, the MOSAIC in BoxMART is run with a time step of 0.01 s to obtain the initial thermodynamic state from the initial condition. After this the model clock is reset to start time and the simulation starts with the solved initial conditions.

For the cases Z2008_CASE13 and Z2008_CASE14, the initial gas concentrations, relative humidity (RH), air pressure and temperature are the same as the corresponding cases as shown in Table 3 of Zaveri et al. (2008). However, the particle size distribution and composition mass distribution were not described explicitly in Zaveri et al. (2008), and therefore in this study these parameters were estimated as faithfully as possible. In both cases Z2008_CASE13 and Z2008_CASE14, 100 size bins were applied, with geometric mean diameter as 5 nm in the smallest size bin and 12 μm in the largest size bin. The number size distribution is the superposition of three lognormal modes with geometric mean diameters 10 nm, 100 nm, and 2 μm, geometric standard deviations 1.5, 1.7 and 1.8, as well as total number concentrations 5.0×10^{10} # m^{-3}, 1.2×10^{9} # m^{-3}, and 6.0×10^{5} # m^{-3}, respectively. Initially, the particles in Aitken and accumulation modes (5 nm to 1 μm) contain NH_4^+ and SO_4^{2-} with a molar ratio of 2:1, and the particles in the coarse mode (1 μm to 12 μm) contain Na^+ and Cl^- with a molar ratio of 1:1. The simulation time step is 60 seconds. It should be noted that the transfer of particles between size bins is calculated with the moving section method in Zaveri et al. (2008) instead of stationary section method used here.

3.10.1 Case Z2008_CASE13

In Z2008_CASE13, the initial ions in the particles form solids $(NH_4)_2SO_4$(s) and NaCl(s) quickly after the initial 0.01 s thermodynamic step under low RH of 30%. Our simulation results agree generally well with that in Zaveri et al. (2008), some apparent differences are discussed below. In our simulation after 5 minutes, the particles smaller than 30 nm are almost removed, while the other larger Aitken mode particles grow quickly (Figs. 9c and 9d). This is slightly different from the results in Zaveri et al. (2008), where all the Aitken mode particles grow more evenly. After 10 hours, our simulation results show more diffusion so that the Aitken and accumulation modes start to merge with each other, and particles smaller than 30 nm are still found (Figs. 9e and 9f). Another difference is the abrupt peak of Na_2SO_4 at around 1 μm in our simulation due to numerical diffusion of stationary method (Figs. 9d and 9f). Because of the diffusion around 1 μm, the particles containing NH_4^+ and the ones containing Cl^- can meet to form NH_4Cl(s) (Fig. 9d). The concentrations of gaseous NH_3 and HCl are higher than HNO_3 after 10 hours, while in Zaveri et al. (2008) their concentrations are nearly the same (Fig. 9g). This could result from that more

https://doi.org/10.5194/egusphere-2026-2381
Preprint. Discussion started: 20 May 2026

small particles exist in our simulation which uptake less NH_3 and HCl. In the other hand, HNO_3 condenses onto particles over the whole size range including coarse particles, so it is not affected by the numerical diffusion as much as the other two gases. In summary, most of the differences between our results and that in Zaveri et al. (2008) can be explained by the differences between stationary section method and moving section method. We also tested Z2008_CASE13 with the original MOSAIC version which has a typo in the Kelvin factor calculation function, and found that it showed nearly the same results. However, this typo affects the phase states of small particles in Z2008_CASE14 which will be shown below.

3.10.2 Case Z2008_CASE14

Our simulation results of Z2008_CASE14_OLD with original Kelvin calculation function agree well with that in Zaveri et al. (2008). And the differences between them are similar with that in Z2008_CASE13, which results from the numerical diffusion of the stationary section method (Figs. 10c and 10d, 10e and 10f). Besides, the number concentration of HNO_3 is slightly lower than HCl, and the NH_3 concentration decreases with oscillation after around 3 hours (Fig. 10g). And Fig. 10h shows that the pH value of particles smaller than 1 μm is not a constant as in Zaveri et al. (2008) after 10 hours. Instead, it is more acidic in Aitken mode and less acidic in accumulation mode.

In Z2008_CASE14_NEW with corrected Kelvin calculation function, the results are similar for particles larger than 100 nm (Figs. 11c, 11d, 11e, 11f, and 11h). However, the most noticable difference is that the particles smaller than 25 nm are solid containing $(NH_4)_2SO_4$(s) and NH_4NO_3(s) despite of high RH of 85%. This results from how Kelvin factor is calculated in two cases. The Kelvin factor in the original version is nearly the same for all the particles with values close to 1, the maximum value for smallest particles (5 nm) is 1.04. While in the new version the Kelvin factor is much larger for smaller particles, and the maximum value for smallest particles is 1.58. This makes water activity (a_w) apparently smaller than RH in the new version according to Eq. 1 in Zaveri et al. (2008), which is 0.81 for smallest particles in the old version and 0.54 in the new version, respectively. Therefore, the growth factor after 10 hours in Z2008_CASE14_OLD is larger than that in Z2008_CASE14_NEW for Aitken mode particles (Fig. 12). Here the diameters in the discussion refer to dry diameters. The relative difference between a_w in wet diameter and a_w in dry diameter is less than 5%, so the discussion here also refers to a_w in dry diameter. Additionally, in the case Z2008_CASE14_NEW, more particles smaller than 30 nm still exist after 5 minutes (Fig. 11c and 11d), and the separation between Aitken mode particles and accumulation mode particles is much more obvious after 10 hours (Fig. 11e and 11f). The pH value also shows sharper change at 100 nm compared to that in Z2008_CASE14_OLD.

In summary, the simulation results in Z2008_CASE14_OLD agree well with that in Zaveri et al. (2008), and the differences can be explained similarly as for Z2008_CASE13. Moreover, the Kelvin effect plays a more significant role here since it decides the phase states of small particles. With the corrected version of Kelvin calculation function in Z2008_CASE14_NEW, the small particles become solid even under a high RH (85%) condition. However, Cheng et al. (2015) proposed that the solid particles would transfer to liquid below a critical diameter, typically around 20 nm. This indicates that more comprehensive mechanisms are needed in simulating particle phase state and transfer correctly.

https://doi.org/10.5194/egusphere-2026-2381
Preprint. Discussion started: 20 May 2026

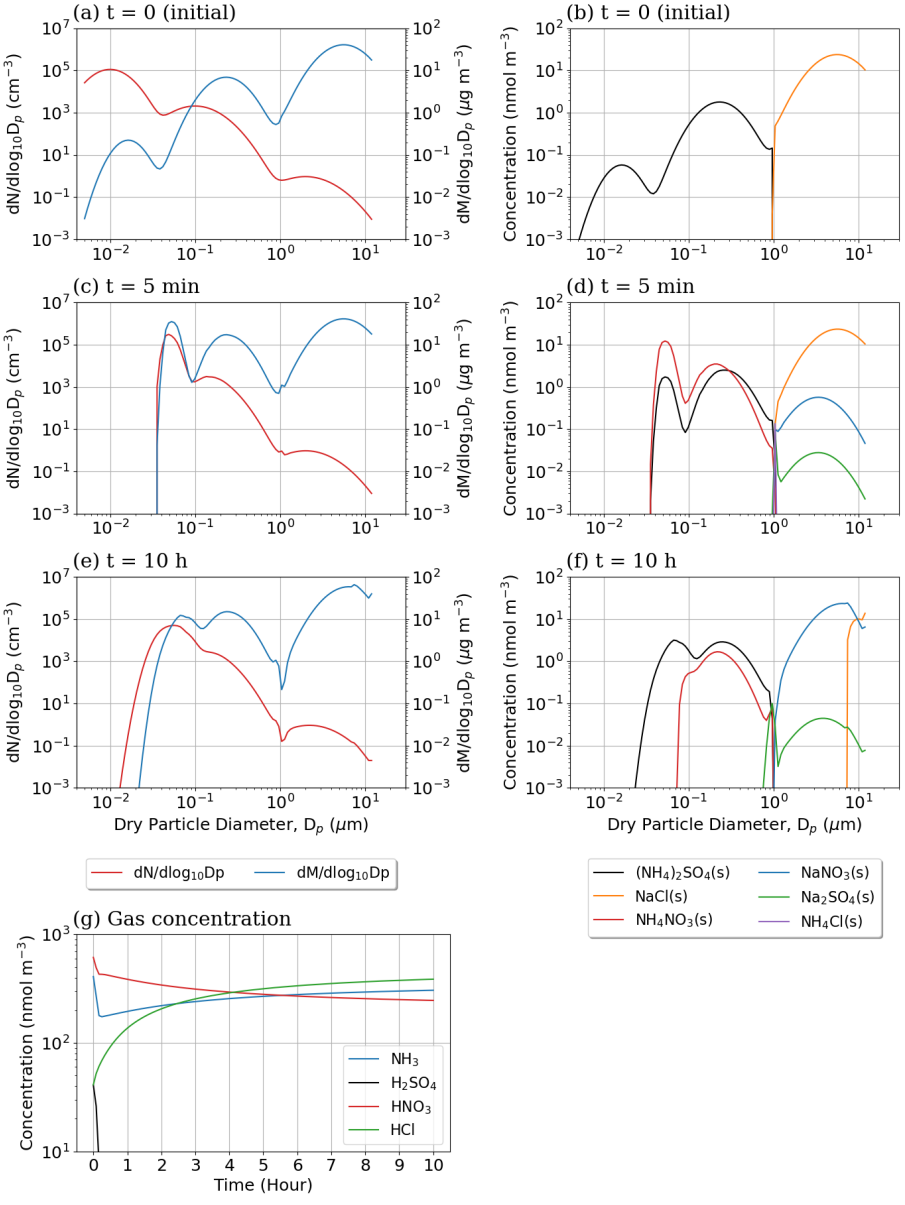

Figure 9. Initial conditions and simulation results of case Z2008_CASE13, (a) The initial conditions, (c) simulation results at 5 minutes and (e) at 10 hours of particle number size distribution and particle mass size distribution. (b) The initial conditions, (d) simulation results at 5 minutes and (f) at 10 hours of molar concentrations of particle phase species in different size bins. (g) Time series of molar concentrations of gaseous species.

https://doi.org/10.5194/egusphere-2026-2381
Preprint. Discussion started: 20 May 2026

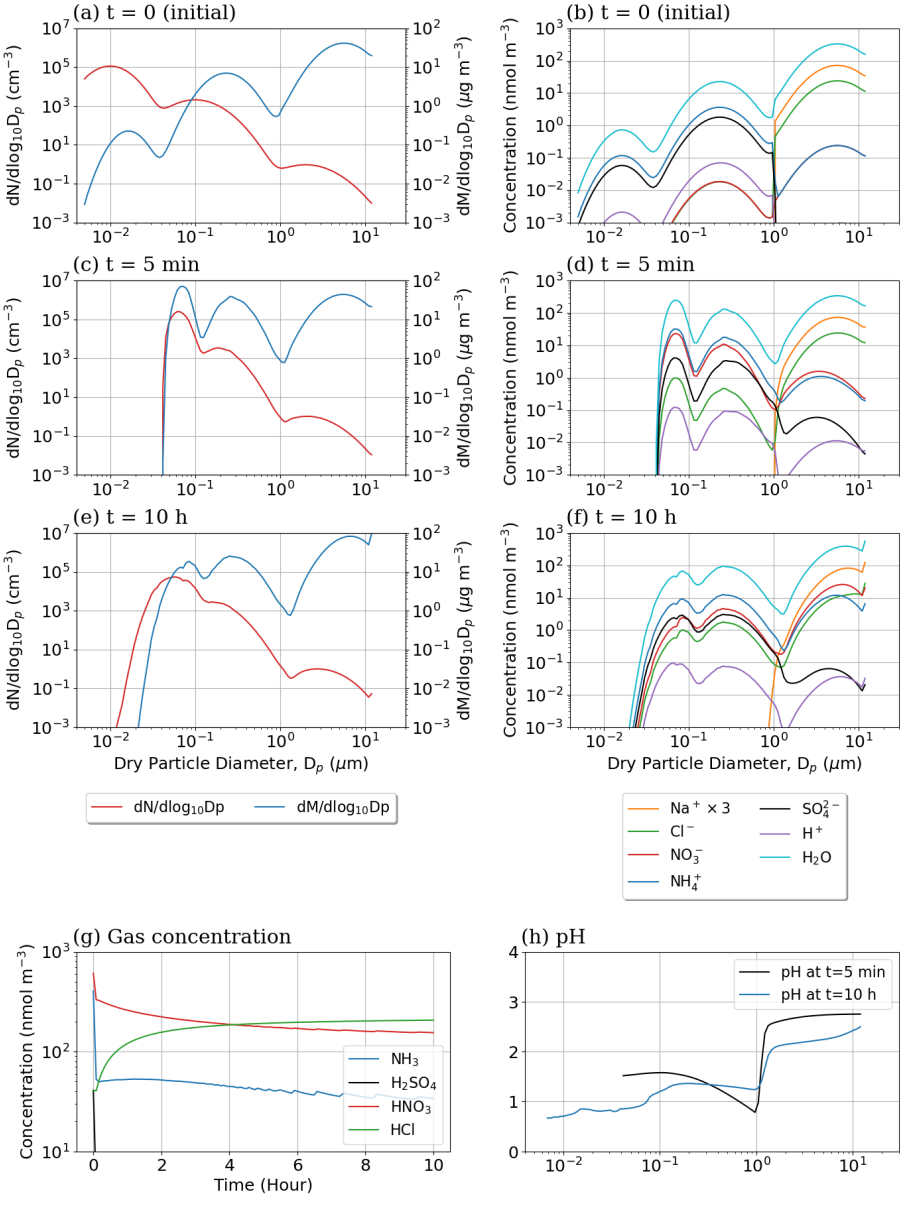

Figure 10. Same as Fig. 9 except for the case Z2008_CASE14_OLD with original Kelvin calculation function. Additionally, the pH size distribution at 5 minutes and 10 hours are shown in (h).

4 Summary and outlook

In this study, a new chemistry and aerosol box model BoxMART (Box Model for Atmospheric Research and Teaching) was introduced, which was aimed for both research simulations and teaching of chemical and aerosol dynamic processes in the

https://doi.org/10.5194/egusphere-2026-2381
Preprint. Discussion started: 20 May 2026

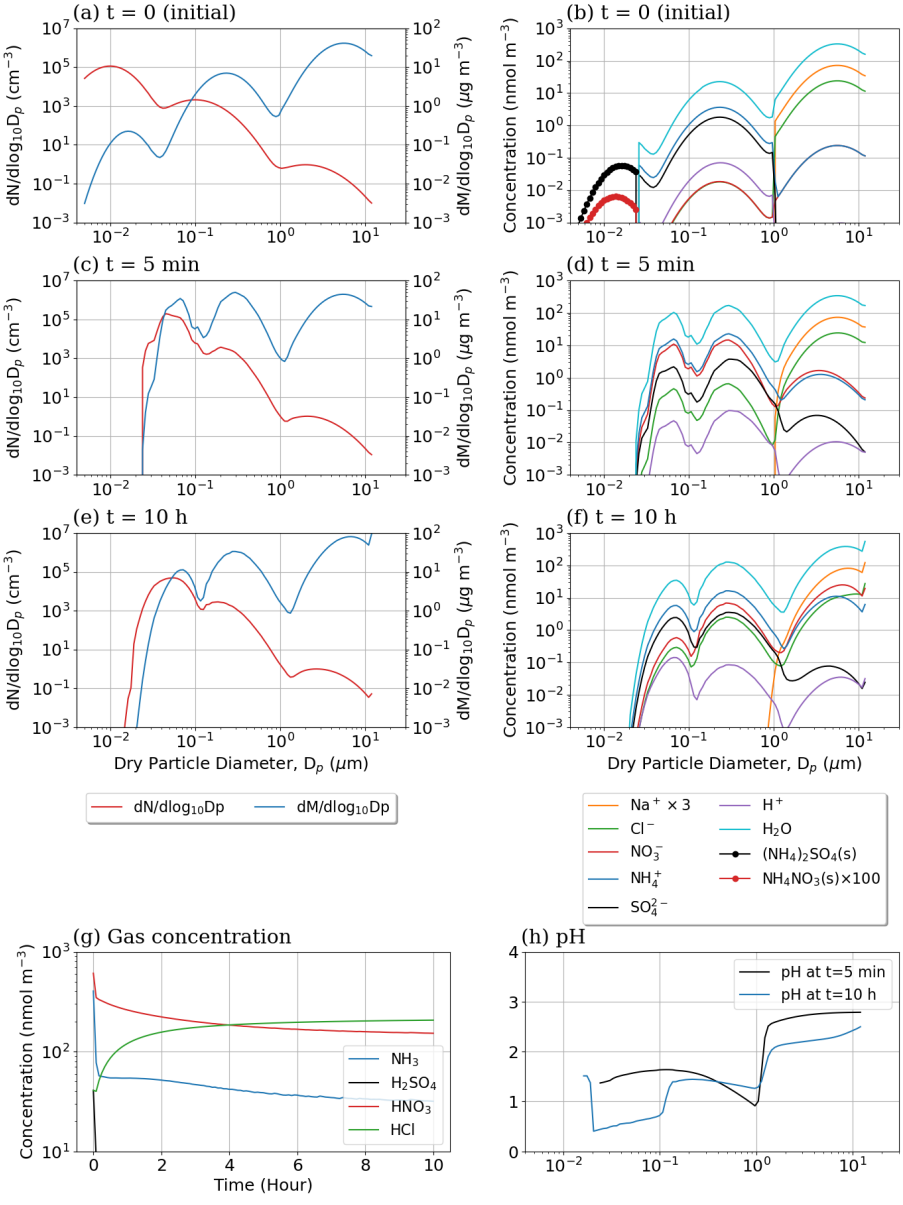

Figure 11. Same as Fig. 10 except for the case Z2008_CASE14_NEW with corrected Kelvin calculation function.

atmosphere. The model of current version has integrated gas-phase chemistry, particle condensation and growth, particle coagulation, as well as aerosol thermodynamic equilibrium process.

In order to evaluate the model performance, 10 benchmark cases or case sets from previous studies were revised and tested, focusing on condensation, dissolution, evaporation, coagulation and aerosol thermodynamic processes. The input and configuration of each simulation case were described in detail. The lack of simulation configuration information was supplemented

https://doi.org/10.5194/egusphere-2026-2381
Preprint. Discussion started: 20 May 2026

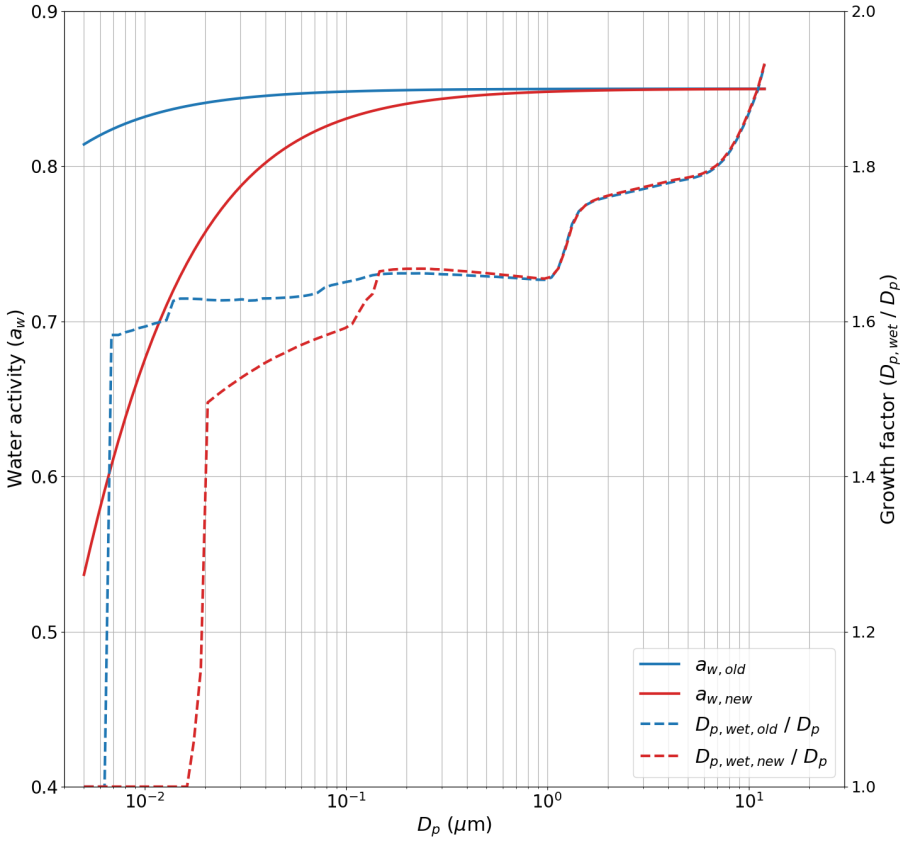

Figure 12. Size distributions of water activities in Z2008_CASE14_OLD (solid blue) and Z2008_CASE14_NEW (solid red). Size distributions of growth factors at 10 hours in Z2008_CASE14_OLD (dahsed blue) and Z2008_CASE14_NEW (dahsed red).

according to the description in corresponding studies, theoretical calculation or numerical experiment trials. The typos in previous studies, if existed, were checked and fixed. All of the efforts were made to make sure that the benchmark simulation cases in this study are repeatable not only with BoxMART, but also with other atmospheric models. Moreover, different processes were verified in different benchmark cases, which is valuable for future model development.

The APC and APD for condensational and dissolutional growth processes were tested in J1997_APC_TEST and J1997_APD_TEST cases. The coagulation process itself was tested in J1994_CASE1, J1994_CASE23, J1994_CASE4, and J1994_CASE5. The condensational growth was tested in JT1995_CASE1, JT1995_CASE2, and JT1995_CASE3 with/without coagulation process. And finally, the aerosol thermodynamic processes were tested in the case set Z2008_CASE. Among them, the combination of condensational growth, coagulation and aerosol thermodynamic process were tested in Z2008_CASE13 and Z2008_CASE14. The simulation results of the case Z2008_CASE14 have shown that small particles can stay in solid state even under high RH value (85%) if their Kelvin factors are large enough.

https://doi.org/10.5194/egusphere-2026-2381
Preprint. Discussion started: 20 May 2026

The current version of the model mainly focuses on the theoretical simulation cases, but it provides a solid base for future development. Future work includes simulating chamber experiments, which requires implementing more mechanisms, including, e.g., wall losses of gases and particles, dilution due to flow rate, multiphase chemical reactions, new particle formation, etc. Furthermore, the cloud related processes will also be considered, e.g., the calculation of cloud condensation nuclei (CCN), cloud droplet formation, etc. As more benchmark simulation cases related to real experiments are added, BoxMART will become a more and more valuable model tool for both research and teaching.

Code availability. The version used in this study has been uploaded to Zenodo (https://doi.org/10.5281/zenodo.19591193, last accessed 28.04.2026; Zhou et al., 2026). The newest version will be updated in the gitlab repository of the University of Helsinki Version Control System (https://version.helsinki.fi), and can be obtained upon request to Putian Zhou (putian.zhou@helsinki.fi).

Author contributions. PZ created and developed the BoxMART model. PZ and ZC designed the simulation cases and ran the simulations. PZ analysed simulation results. PZ wrote the manuscript with input from all other co-authors.

Competing interests. The authors declare that they have no conflict of interest.

Acknowledgements. PZ would like to acknowledge the European Commission Horizon Europe project FOCI (grant agreement no. 101056783) and DORA project (Väisälä Project Grant). PZ would like to thank discussion and communication with Mark Jacobson, Matthias Karl, and Rahul Zaveri. ZF would like to thank National Natural Science Foundation of China (22306002). We thank city of Lahti for financial support. The work was supported by ACCC Flagship funded by the Academy of Finland (grant number 337549). We wish to acknowledge CSC - IT Center for Science, Finland, for computational resources.

https://doi.org/10.5194/egusphere-2026-2381
Preprint. Discussion started: 20 May 2026

Appendix A: Setup of particle bin structure

There are eight methods to setup the particle bin structure aiming for various simulation cases. The explanation is shown below:

1. The bins are set to a logarithmic sequence with constant difference $\mathrm{d}\log_{10}(D_p)$. The input parameters are number of bins (N), particle diameter at the lower bound of the smallest size bin ($D_{p,1,l}$), and particle diameter at the upper bound of the largest size bin ($D_{p,N,u}$). So the particle diameter representing the size bin i ($D_{p,i}$, $i = 1, 2, \ldots, N$), which is the geometric mean of the lower bound diameter and the upper bound diameter, can be calculated as:

$$\mathrm{d}\log_{10} D_p = (\log_{10} D_{p,N,u} - \log_{10} D_{p,1,l})/N \tag{A1}$$

$$\log_{10} D_{p,i} = \log_{10} D_{p,1,l} + (i - 0.5) \cdot \mathrm{d}\log_{10} D_p \tag{A2}$$

$$\log_{10} D_{p,i,l} = \log_{10} D_{p,1,l} + (i - 1) \cdot \mathrm{d}\log_{10} D_p \tag{A3}$$

$$\log_{10} D_{p,i,u} = \log_{10} D_{p,1,l} + i \cdot \mathrm{d}\log_{10} D_p \tag{A4}$$

2. This method is the same as method 1 but the input parameters are particle diameters representing the smallest ($D_{p,1}$) and largest size bins ($D_{p,N}$), respectively. And the other parameters are calculated as:

$$\mathrm{d}\log_{10} D_p = (\log_{10} D_{p,N} - \log_{10} D_{p,1})/(N - 1) \tag{A5}$$

$$\log_{10} D_{p,i} = \log_{10} D_{p,1} + (i - 1) \cdot \mathrm{d}\log_{10} D_p \tag{A6}$$

$$\log_{10} D_{p,i,l} = \log_{10} D_{p,1} + (i - 0.5) \cdot \mathrm{d}\log_{10} D_p \tag{A7}$$

$$\log_{10} D_{p,i,u} = \log_{10} D_{p,1} + (i + 0.5) \cdot \mathrm{d}\log_{10} D_p \tag{A8}$$

3. Manually set size distribution with input parameters being $N + 1$ size bin bounds $D_{p,i,l}$ and $D_{p,i,u}$. Other parameters are calculated as:

$$\mathrm{d}\log_{10} D_{p,i} = \log_{10} D_{p,i,u} - \log_{10} D_{p,i,l} \tag{A9}$$

$$\log_{10} D_{p,i} = 0.5 \cdot (\log_{10} D_{p,i,l} + \log_{10} D_{p,i,u}) \tag{A10}$$

4. Manually set size distribution with input parameters being N size bin diameters. Other parameters are calculated as:

$$\log_{10} D_{p,i,l} = 0.5 \cdot (\log_{10} D_{p,i-1} + \log_{10} D_{p,i}), \quad i = 2, \ldots, N \tag{A11}$$

$$\log_{10} D_{p,i,u} = 0.5 \cdot (\log_{10} D_{p,i} + \log_{10} D_{p,i+1}), \quad i = 1, \ldots, N - 1 \tag{A12}$$

$$\log_{10} D_{p,1,l} = 2 \cdot \log_{10} D_{p,1} - \log_{10} D_{p,1,u} \tag{A13}$$

$$\log_{10} D_{p,N,u} = 2 \cdot \log_{10} D_{p,N} - \log_{10} D_{p,N,l} \tag{A14}$$

$$\mathrm{d}\log_{10} D_{p,i} = \log_{10} D_{p,i,u} - \log_{10} D_{p,i,l} \tag{A15}$$

5. The first n_1 size bins in this size distribution have a constant volume ratio V_{r1}, and the rest of the bins ($N - n_1$) have another constant volume ratio V_{r2}. Here the volume ratio in a size bin is equal to the ratio between the volumes at

https://doi.org/10.5194/egusphere-2026-2381
Preprint. Discussion started: 20 May 2026

upper bound and lower bound. In this case, the value $\mathrm{d}\log_{10} D_p$ is the same in the size bins with the same volume ratio. Therefore, this size distribution can also be represented by a logarithmic sequence of particle diameters. In this method, the input parameters are $V_{1,l}$, V_{r1}, V_{r2}, n_1 and N, From this we can get:

$$V_{i,u} = \begin{cases} V_{1,l} V_{r1}^{i}, & i = 1, \ldots, n1 \\ V_{n1,u} V_{r2}^{i-n1}, & i = n1+1, \ldots, N \end{cases} \tag{A16}$$

$$V_{i,l} = V_{i-1,u}, \quad i = 2, \ldots, N \tag{A17}$$

Then we can obtain $D_{p,i}$, $D_{p,i,l}$ and $D_{p,i,u}$.

6. This size distribution is the same as the one above, but the input parameters are V_1, V_{r1}, V_{r2}, n_1 and N. Because

$$\log_{10} D_{p,i} = 0.5 \cdot (\log_{10} D_{p,i,l} + \log_{10} D_{p,i,u}) \tag{A18}$$

which deduces:

$$\log_{10} V_i = 0.5 \cdot (\log_{10} V_{i,l} + \log_{10} V_{i,u}) \tag{A19}$$

$$\frac{V_{i,u}}{V_i} = \frac{V_i}{V_{i,l}} \tag{A20}$$

$$V_r = \frac{V_{i,u}}{V_{i,l}} = \left(\frac{V_i}{V_{i,l}} \right)^2 \tag{A21}$$

So we can get $V_{1,l}$ from V_1 by:

$$V_{1,l} = \frac{V_1}{\sqrt{V_{r1}}} \tag{A22}$$

then all the following calculation is the same as that in method 5.

7. In this size distribution the volumes in the first n_m size bins are multiplication of monomers, and in the rest of the bins the volumes follow varied volume ratios. The first size bin contains monomers with particle diameter as $D_{p,1}$. And the volume ratios in the rest of the bins change linearly from $V_{r,min}$ to $V_{r,max}$. This size distribution has high resolution in the small bins and appropriate number of large bins. The input parameters are $D_{p,1}$, n_m, $V_{r,max}$ and N. The $V_{r,min}$ is assumed as a continuation of monomer size bins:

$$V_{r,min} = \frac{n_m + 1}{n_m} \tag{A23}$$

So the volume of the rest bins are calculated as:

$$\Delta V_r = \frac{V_{r,max} - V_{r,min}}{N - n_m - 1}, \quad N > n_m + 1 \tag{A24}$$

$$V_i = [V_{r,min} + (i - n_m - 1) \cdot \Delta V_r] \cdot V_{i-1}, \quad i = n_m + 1, \ldots, N \tag{A25}$$

https://doi.org/10.5194/egusphere-2026-2381
Preprint. Discussion started: 20 May 2026

8. In the methods 5 and 6, there will exist concentration dips in the first several smallest bins considering coagulation process, if the volume ratio is too small. To overcome this deficit, the bin volumes should be set in a slightly different way. In Jacobson et al. (1994), the threshold of the volume ratio, under which the concentration dips occur, is 1.62, which is the volume ratio when first bin volume plus second bin volume is larger then the third bin volume:

$$1 + r > r^2 \tag{A26}$$

where r is used to represent V_r for simplicity, and the volume of the first bin V_1 is divided off from both sides. Here $r > 1$. In the following discussion, we will always divide the V_1 off for simplicity. However, if we consider how the coagulation process is calculated, this criteria is not precise. For example, the smallest combination between two particles are first bin plus first bin instead of first bin plus second bin. In a general case, suppose a size bin alignment: $1, r, r^2, r^3, r^4, ...$, if we want every size bin except the first one can get coagulated particles, all these size ranges shown below must include at least one coagulated particle volume: $(1, r^2), (r, r^3), (r^2, r^4), (r^3, r^5), ...$ And the combined volumes are ordered starting from smallest values as: $2, 1 + r, 2r, r^2 + 1, ...$ Hence, 2 should be in the range of $(1, r^2)$, which means:

$$2 < r^2 \tag{A27}$$

$$r > \sqrt{2} \tag{A28}$$

Then we can derive that $r + 1$ is in the range of (r, r^3), because:

$$r + 1 > r \tag{A29}$$

$$r^3 - (r + 1) = r(r^2 - 1) - 1 > r(2 - 1) - 1 = r - 1 > 0 \tag{A30}$$

And for all the subsequent ranges, e.g., $(r^m, r^{m+2}), m \geq 2$, we can prove that:

$$r^m + 1 > r^m \tag{A31}$$

$$r^{m+2} - (r^m + 1) = r^m(r^2 - 1) - 1 > r^m - 1 > 0 \tag{A32}$$

so at least the coagulation between bin 1 and bin $m + 1$ lies in the range (r^m, r^{m+2}). So the threshold ratio value is $r_c = \sqrt{2}$ instead of 1.62, and when $r > r_c$, all the size bins except the first one will get coagulated particles after interpolation, which can be named as "bin coagulation criteria". When $r \leqslant r_c$, we can construct an alignment of size bins to fulfill the criteria. Different approaches can be applied according to individual needs, here is an example with N size bins: $1, 2, r^m, r^{m+1}, ..., r^{m+N-3}$, Here $m \geqslant 3$ because $r^2 \leqslant 2$, and we need to find m to meet both requirements shown below:

$$r^{m+1} > 3 \tag{A33}$$

$$r^{m+2} - r^m > 1 \tag{A34}$$

For example, for $r = 1.2$, $m = 6$, and we can construct the size bins as: $1, 2, 1.2^6(2.99), 1.2^7(3.58), 1.2^8(4.30), ...$ So the input parameters in this method are $D_{p,1}$, V_r and N.

https://doi.org/10.5194/egusphere-2026-2381
Preprint. Discussion started: 20 May 2026

Appendix B: Cases from Z2008_CASE1 to Z2008_CASE12

From Z2008_CASE1 to Z2008_CASE12, the particles lie in one size bin with the same diameter. In our simulations, the growth of particles are not considered in these cases, so the particles keep their dry diameters while the compositions inside are changing with time. However, we noticed that the smallest particle dry diameter in these cases was 300 nm, indicating that the particle growth can be neglected compared to their size. This is also proved by the simulation results as shown below. The initial conditions of the cases from Z2008_CASE1 to Z2008_CASE12 are the same as the corresponding cases as shown in Table 3 of Zaveri et al. (2008).

The simulation results here are compared with that in Zaveri et al. (2008). The case CASE1 agrees well (Fig. B1a and b). In case CASE2, the gas H_2SO_4 decreases slightly faster (Fig. B1c), and the time variation of NH_4Cl is also plotted which is not shown in Zaveri et al. (2008) (Fig. B1d). In the beginning, Cl^- in the NaCl(s) is replaced by the condensed SO_4^{2-} and NO_3^-. But at the same time NH_4Cl(s) forms when NH_3 condenses, which also uptakes HCl. After that, when more HNO_3 condenses, NH_4Cl(s) is replaced by NH_4NO_3(s) and HCl is evaporated. This also explains the dip in the time variation of HCl concentration (Fig. B1c).

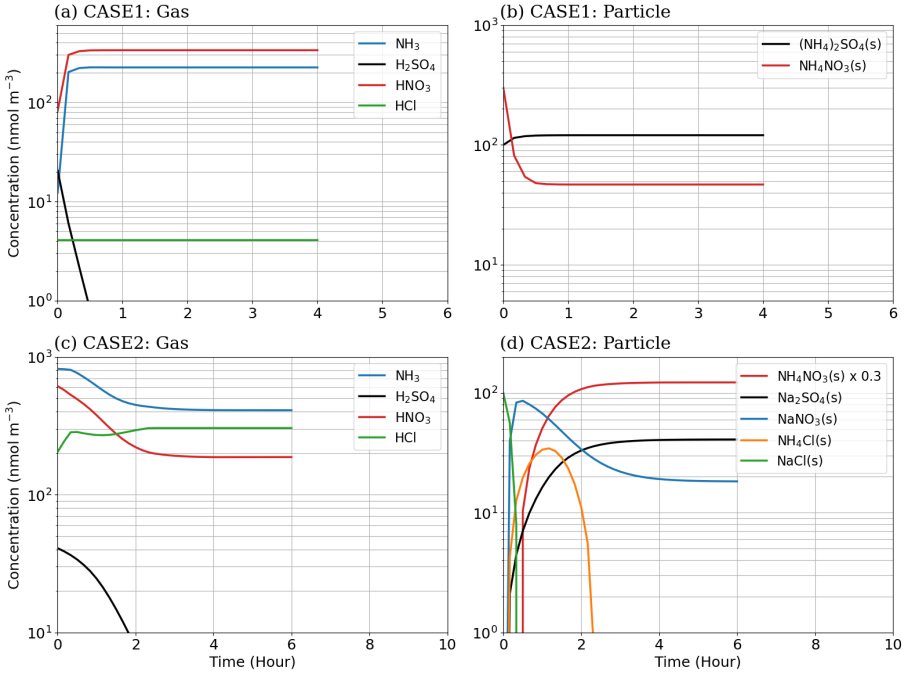

Figure B1. Time series of (a, c) gases and (b, d) particle phase species in cases Z2008_CASE1 and Z2008_CASE2, respectively. The aerosol particles are solid under low RH values (RH=30%) in these cases.

The results of cases CASE4, CASE5, CASE6, CASE7 and CASE9 agree well, a minor difference is that H_2SO_4 condenses slightly faster in CASE5 (Fig. B2, B3c, and B3d). In the case CASE8 with current version of MOSAIC in our simulation,

https://doi.org/10.5194/egusphere-2026-2381
Preprint. Discussion started: 20 May 2026

H_2O, NH_4^+, $(NH_4)_2SO_4$(s) and SO_4^{2-} do not have the dips in the beginning, which seems more reasonable than that in Zaveri et al. (2008) (Fig. B3a and B3b). Because in the original Case 8, during the first several minutes, the concentrations of NH_3 in gas phase and all the NH_4^+-contained species in particle phase are decreasing which violates the mass conservation. This also happens for gaseous H_2SO_4 and particle phase SO_4^{2-}-contained species. Nonetheless, the concentrations of the species in the final equilibrium state agree well.

The RH changes with time in cases CASE11 and CASE12. In our simulation in CASE11, NH_4Cl(s) exists in a short time, while it is not shown at all in the original Case 11 (Fig. B4a and B4b). Otherwise, it agrees well. In CASE12, the equilibrium states agree well (Fig. B4c and B4d). Moreover, the water content decreases as the RH decreases, which results in the decreasing of H^+. However, in our case the other ion species keep their concentrations which indicates enhanced molarities. While in the original Case 12, the molar concentrations of NH_4^+, NO_3^- and Cl^- also decrease with H_2O, corresponding to increasing of their gaseous counterparts NH_3, HNO_3 and HCl. This uncaught feature needs further investigation in future.

https://doi.org/10.5194/egusphere-2026-2381
Preprint. Discussion started: 20 May 2026

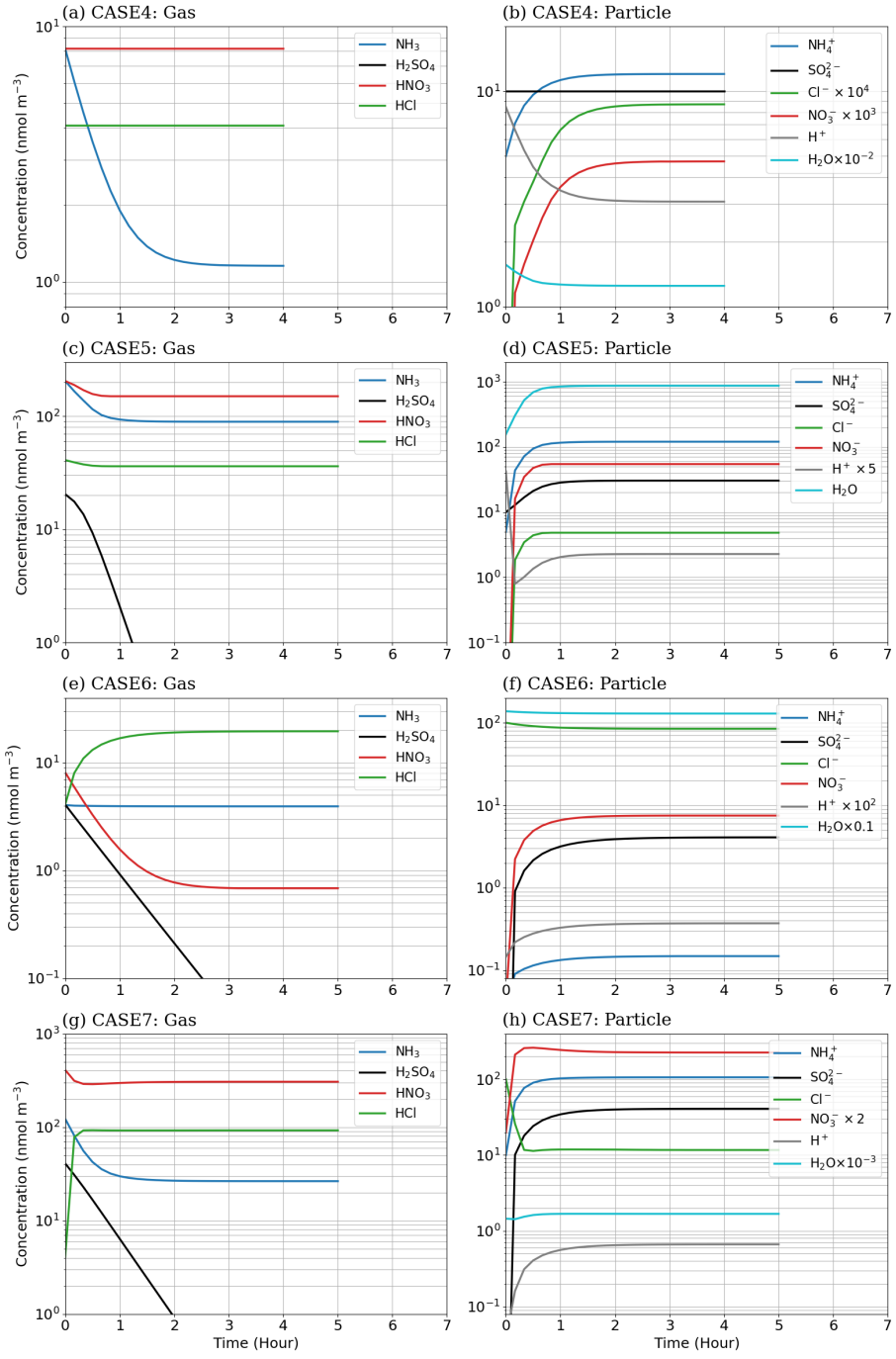

Figure B2. Time series of (a, c, e, g) gases and (b, d, f, h) particle phase species in cases Z2008_CASE4, Z2008_CASE5, Z2008_CASE6, and Z2008_CASE7, respectively. The aerosol particles are liquid under high RH values (RH=85%) in these cases.

https://doi.org/10.5194/egusphere-2026-2381
Preprint. Discussion started: 20 May 2026

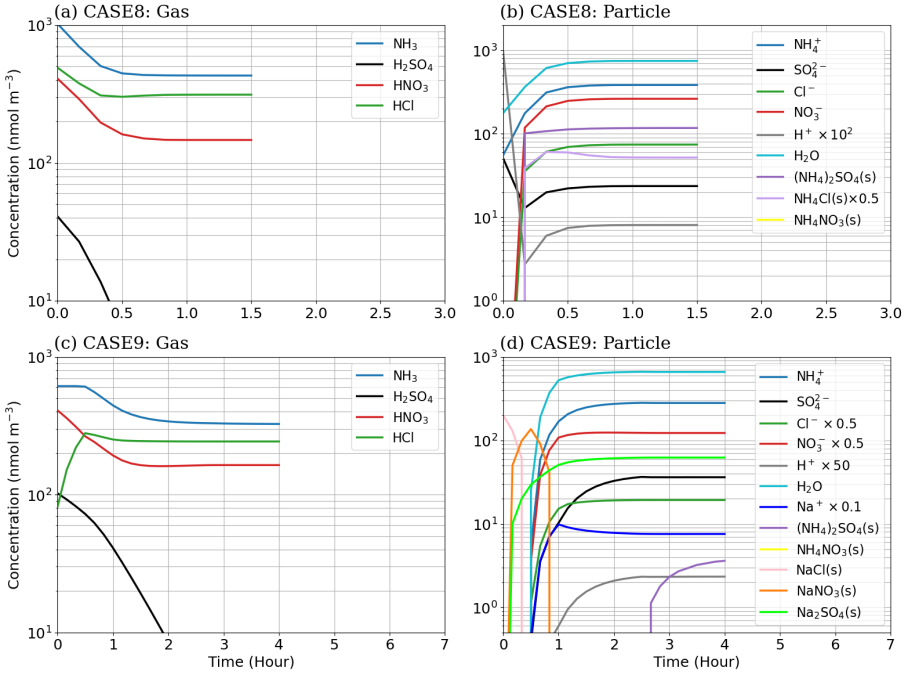

Figure B3. Time series of (a, c) gases and (b, d) particle phase species in cases Z2008_CASE8 and Z2008_CASE9, respectively. The aerosol particles are mixed phase under medium RH values, which is 55% in Z2008_CASE8 and 52% in Z2008_CASE9.

https://doi.org/10.5194/egusphere-2026-2381
Preprint. Discussion started: 20 May 2026

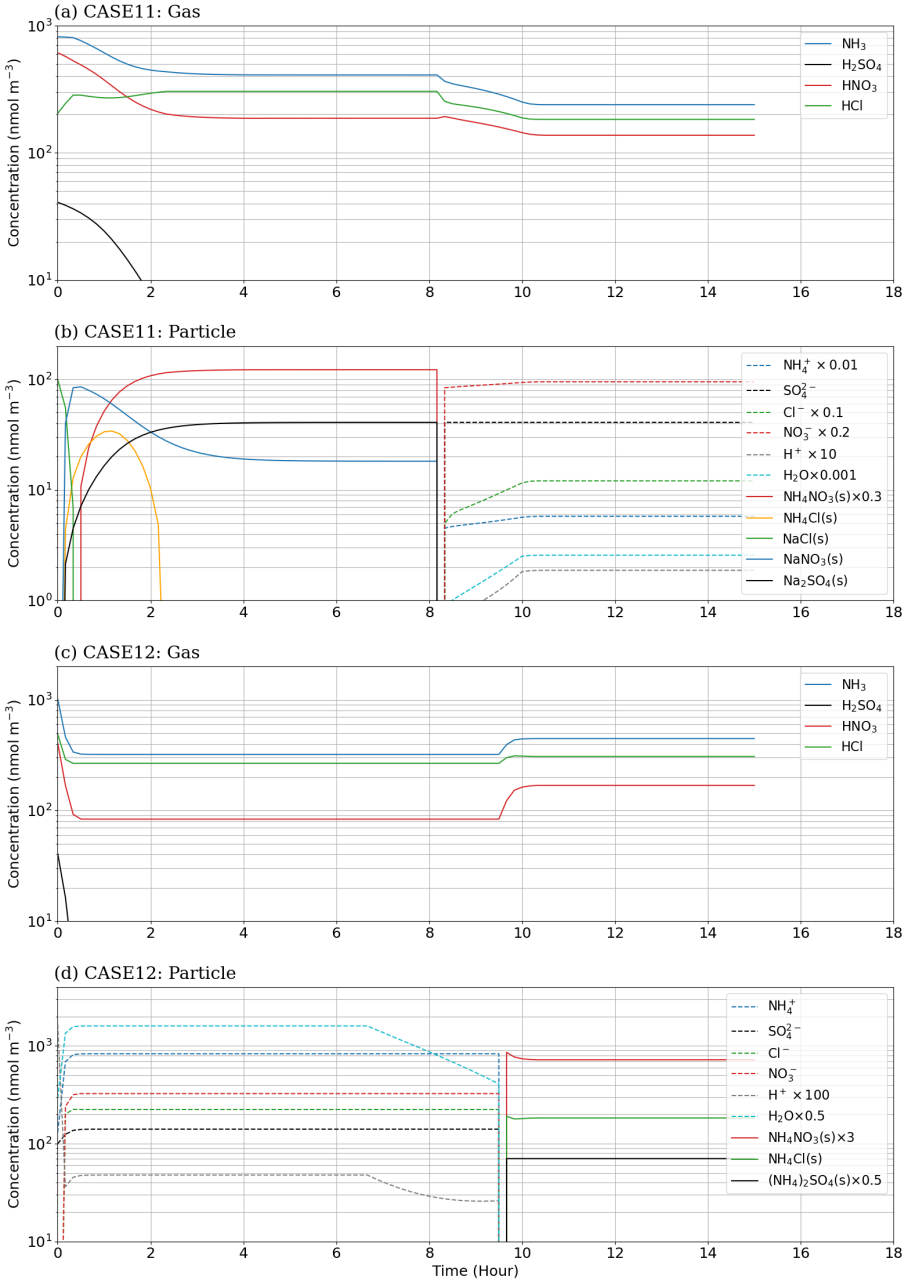

Figure B4. Time series of (a, c) gases and (b, d) particle phase species in cases Z2008_CASE11 and Z2008_CASE12, respectively. In CASE11, the RH values is 30% initially, and starts to increase linearly at 6.67 h to 70% at 10 h. In CASE12, the RH values is 70% initially, and starts to decrease linearly at 6.67 h to 30% at 10 h.

https://doi.org/10.5194/egusphere-2026-2381
Preprint. Discussion started: 20 May 2026

References

Albrecht, B. A.: Aerosols, Cloud Microphysics, and Fractional Cloudiness, Science, 245, 1227–1230, https://doi.org/10.1126/science.245.4923.1227, publisher: American Association for the Advancement of Science, 1989.

Bellouin, N., Quaas, J., Gryspeerdt, E., Kinne, S., Stier, P., Watson-Parris, D., Boucher, O., Carslaw, K. S., Christensen, M., Daniau, A., Dufresne, J., Feingold, G., Fiedler, S., Forster, P., Gettelman, A., Haywood, J. M., Lohmann, U., Malavelle, F., Mauritsen, T., McCoy, D. T., Myhre, G., Mülmenstädt, J., Neubauer, D., Possner, A., Rugenstein, M., Sato, Y., Schulz, M., Schwartz, S. E., Sourdeval, O., Storelvmo, T., Toll, V., Winker, D., and Stevens, B.: Bounding Global Aerosol Radiative Forcing of Climate Change, Reviews of Geophysics, 58, e2019RG000 660, https://doi.org/10.1029/2019RG000660, 2020.

Bhatti, Y. A., Watson-Parris, D., Regayre, L. A., Jia, H., Neubauer, D., Im, U., Svenhag, C., Schutgens, N., Tsikerdekis, A., Nenes, A., Irfan, M., van Diedenhoven, B., Arifi, A., Fu, G., and Hasekamp, O. P.: Uncertainty in aerosol effective radiative forcing from anthropogenic and natural aerosol parameters in ECHAM6.3-HAM2.3, Atmospheric Chemistry and Physics, 26, 269–293, https://doi.org/10.5194/acp-26-269-2026, publisher: Copernicus GmbH, 2026.

Bond, T. C., Doherty, S. J., Fahey, D. W., Forster, P. M., Berntsen, T., DeAngelo, B. J., Flanner, M. G., Ghan, S., Kärcher, B., Koch, D., Kinne, S., Kondo, Y., Quinn, P. K., Sarofim, M. C., Schultz, M. G., Schulz, M., Venkataraman, C., Zhang, H., Zhang, S., Bellouin, N., Guttikunda, S. K., Hopke, P. K., Jacobson, M. Z., Kaiser, J. W., Klimont, Z., Lohmann, U., Schwarz, J. P., Shindell, D., Storelvmo, T., Warren, S. G., and Zender, C. S.: Bounding the role of black carbon in the climate system: A scientific assessment, Journal of Geophysical Research: Atmospheres, 118, 5380–5552, https://doi.org/10.1002/jgrd.50171, _eprint: https://agupubs.onlinelibrary.wiley.com/doi/pdf/10.1002/jgrd.50171, 2013.

Boy, M., Hellmuth, O., Korhonen, H., Nilsson, E. D., ReVelle, D., Turnipseed, A., Arnold, F., and Kulmala, M.: MALTE–model to predict new aerosol formation in the lower troposphere, Atmos. Chem. Phys., 6, 4499–4517, 2006.

Boy, M., Sogachev, A., Lauros, J., Zhou, L., Guenther, A., and Smolander, S.: SOSA–a new model to simulate the concentrations of organic vapours and sulphuric acid inside the ABL – Part 1: Model description and initial evaluation, Atmos. Chem. Phys., 11, 43–51, 2011.

Cheng, Y., Su, H., Koop, T., Mikhailov, E., and Pöschl, U.: Size dependence of phase transitions in aerosol nanoparticles, Nat Commun, 6, https://doi.org/https://doi.org/10.1038/ncomms6923, 2015.

Clegg, S. L., Seinfeld, J. H., and Brimblecombe, P.: Thermodynamic modelling of aqueous aerosols containing electrolytes and dissolved organic compounds, Journal of Aerosol Science, 32, 713–738, https://doi.org/10.1016/S0021-8502(00)00105-1, 2001.

Clegg, S. L., Kleeman, M. J., Griffin, R. J., and Seinfeld, J. H.: Effects of uncertainties in the thermodynamic properties of aerosol components in an air quality model – Part 1: Treatment of inorganic electrolytes and organic compounds in the condensed phase, Atmospheric Chemistry and Physics, 8, 1057–1085, https://doi.org/10.5194/acp-8-1057-2008, publisher: Copernicus GmbH, 2008.

Clusius, P., Xavier, C., Pichelstorfer, L., Zhou, P., Olenius, T., Roldin, P., and Boy, M.: Atmospherically Relevant Chemistry and Aerosol box model - ARCA box (version 1.2), Geoscientific Model Development, 15, 7257–7286, https://doi.org/10.5194/gmd-15-7257-2022, publisher: Copernicus GmbH, 2022.

Forster, P., Storelvmo, T., Armour, K., Collins, W., Dufresne, J.-L., Frame, D., Lunt, D., Mauritsen, T., Palmer, M., Watanabe, M., Wild, M., and Zhang, H.: 2021: The Earth's Energy Budget, Climate Feedbacks, and Climate Sensitivity. In Climate Change 2021: The Physical Science Basis. Contribution of Working Group I to the Sixth Assessment Report of the Intergovernmental Panel on Climate Change, pp. 923–1054, Cambridge University Press, Cambridge, United Kingdom and New York, NY, USA, https://doi.org/doi:10.1017/9781009157896.009, 2021.

https://doi.org/10.5194/egusphere-2026-2381
Preprint. Discussion started: 20 May 2026

Fountoukis, C. and Nenes, A.: ISORROPIA II: a computationally efficient thermodynamic equilibrium model for K+ - Ca2+ - Mg2+ - NH4+ - Na+ - SO42- - NO3- - Cl- - H2O aerosols, Atmospheric Chemistry and Physics, 7, 4639–4659, https://doi.org/10.5194/acp-7-4639-2007, publisher: Copernicus GmbH, 2007.

Fu, Z., Ma, F., Liu, Y., Yan, C., Huang, D., Chen, J., Elm, J., Li, Y., Ding, A., Pichelstorfer, L., Xie, H.-B., Nie, W., Francisco, J. S., and Zhou, P.: An overlooked oxidation mechanism of toluene: computational predictions and experimental validations, Chem. Sci., 14, 13 050–13 059, https://doi.org/10.1039/D3SC03638C, 2023.

Gelbard, F. and Seinfeld, J. H.: Numerical solution of the dynamic equation for particulate systems, Journal of Computational Physics, 28, 357–375, https://doi.org/https://doi.org/10.1016/0021-9991(78)90058-X, 1978.

Gryspeerdt, E., Goren, T., Sourdeval, O., Quaas, J., Mülmenstädt, J., Dipu, S., Unglaub, C., Gettelman, A., and Christensen, M.: Constraining the aerosol influence on cloud liquid water path, Atmospheric Chemistry and Physics, 19, 5331–5347, https://doi.org/10.5194/acp-19-5331-2019, publisher: Copernicus GmbH, 2019.

Hodas, N., Zuend, A., Mui, W., Flagan, R. C., and Seinfeld, J. H.: Influence of particle-phase state on the hygroscopic behavior of mixed organic–inorganic aerosols, Atmospheric Chemistry and Physics, 15, 5027–5045, https://doi.org/10.5194/acp-15-5027-2015, publisher: Copernicus GmbH, 2015.

Jacobson, M. Z.: Numerical Techniques to Solve Condensational and Dissolutional Growth Equations When Growth is Coupled to Reversible Reactions, Aerosol Science and Technology, 27, 491–498, https://doi.org/10.1080/02786829708965489, 1997.

Jacobson, M. Z.: Studying the effects of calcium and magnesium on size-distributed nitrate and ammonium with EQUISOLV II, Atmospheric Environment, 1999.

Jacobson, M. Z.: Analysis of aerosol interactions with numerical techniques for solving coagulation, nucleation, condensation, dissolution, and reversible chemistry among multiple size distributions, Journal of Geophysical Research, 107, https://doi.org/10.1029/2001JD002044, 2002.

Jacobson, M. Z.: Fundamentals of Atmospheric Modeling, Cambridge University Press, 2 edn., 2005.

Jacobson, M. Z. and Turco, R. P.: Simulating Condensational Growth, Evaporation, and Coagulation of Aerosols Using a Combined Moving and Stationary Size Grid, Aerosol Science and Technology, 22, 73–92, https://doi.org/10.1080/02786829408959729, 1995.

Jacobson, M. Z., Turco, R. P., Jensen, E. J., and Toon, O. B.: Modeling coagulation among particles of different composition and size, Atmospheric Environment, 28, 1327–1338, https://doi.org/10.1016/1352-2310(94)90280-1, 1994.

Kakavas, S., Pandis, S. N., and Nenes, A.: ISORROPIA-Lite: A Comprehensive Atmospheric Aerosol Thermodynamics Module for Earth System Models, Tellus B: Chemical and Physical Meteorology, 74, https://doi.org/10.16993/tellusb.33, 2022.

Karl, M., Pirjola, L., Grönholm, T., Kurppa, M., Anand, S., Zhang, X., Held, A., Sander, R., Dal Maso, M., Topping, D., Jiang, S., Kangas, L., and Kukkonen, J.: Description and evaluation of the community aerosol dynamics model MAFOR v2.0, Geoscientific Model Development, 15, 3969–4026, https://doi.org/10.5194/gmd-15-3969-2022, publisher: Copernicus GmbH, 2022.

Li, J., Carlson, B. E., Yung, Y. L., Lv, D., Hansen, J., Penner, J. E., Liao, H., Ramaswamy, V., Kahn, R. A., Zhang, P., Dubovik, O., Ding, A., Lacis, A. A., Zhang, L., and Dong, Y.: Scattering and absorbing aerosols in the climate system, Nature Reviews Earth & Environment, 3, 363–379, https://doi.org/10.1038/s43017-022-00296-7, publisher: Nature Publishing Group, 2022.

Moise, T., Flores, J. M., and Rudich, Y.: Optical Properties of Secondary Organic Aerosols and Their Changes by Chemical Processes, Chemical Reviews, 115, 4400–4439, https://doi.org/10.1021/cr5005259, 2015.

O'Meara, S. P., Xu, S., Topping, D., Alfarra, M. R., Capes, G., Lowe, D., Shao, Y., and McFiggans, G.: PyCHAM (v2.1.1): a Python box model for simulating aerosol chambers, Geoscientific Model Development, 14, 675–702, https://doi.org/10.5194/gmd-14-675-2021, 2021.

https://doi.org/10.5194/egusphere-2026-2381
Preprint. Discussion started: 20 May 2026

Pugsley, G., Gryspeerdt, E., and Nair, V.: Cloud fraction response to aerosol driven by nighttime processes, Proceedings of the National Academy of Sciences of the United States of America, 122, e2509949 122, https://doi.org/10.1073/pnas.2509949122, 2025.

Pye, H. O. T., Liao, H., Wu, S., Mickley, L. J., Jacob, D. J., Henze, D. K., and Seinfeld, J. H.: Effect of changes in climate and emissions on future sulfate-nitrate-ammonium aerosol levels in the United States, Journal of Geophysical Research: Atmospheres, 114, https://doi.org/10.1029/2008JD010701, _eprint: https://agupubs.onlinelibrary.wiley.com/doi/pdf/10.1029/2008JD010701, 2009.

Riemer, N., Ault, A. P., West, M., Craig, R. L., and Curtis, J. H.: Aerosol Mixing State: Measurements, Modeling, and Impacts, Reviews of Geophysics, 57, 187–249, https://doi.org/10.1029/2018RG000615, _eprint: https://agupubs.onlinelibrary.wiley.com/doi/pdf/10.1029/2018RG000615, 2019.

Roldin, P., Eriksson, A. C., Nordin, E. Z., Hermansson, E., Mogensen, D., Rusanen, A., Boy, M., Swietlicki, E., Svenningsson, B., Zelenyuk, A., and Pagels, J.: Modelling non-equilibrium secondary organic aerosol formation and evaporation with the aerosol dynamics, gas- and particle-phase chemistry kinetic multilayer model ADCHAM, Atmospheric Chemistry and Physics, 14, 7953–7993, https://doi.org/10.5194/acp-14-7953-2014, publisher: Copernicus GmbH, 2014.

Saleh, R., Marks, M., Heo, J., Adams, P. J., Donahue, N. M., and Robinson, A. L.: Contribution of brown carbon and lensing to the direct radiative effect of carbonaceous aerosols from biomass and biofuel burning emissions, Journal of Geophysical Research: Atmospheres, 120, 10,285–10,296, https://doi.org/10.1002/2015JD023697, _eprint: https://agupubs.onlinelibrary.wiley.com/doi/pdf/10.1002/2015JD023697, 2015.

Sand, M., Samset, B. H., Myhre, G., Gliß, J., Bauer, S. E., Bian, H., Chin, M., Checa-Garcia, R., Ginoux, P., Kipling, Z., Kirkevåg, A., Kokkola, H., Le Sager, P., Lund, M. T., Matsui, H., van Noije, T., Olivié, D. J. L., Remy, S., Schulz, M., Stier, P., Stjern, C. W., Takemura, T., Tsigaridis, K., Tsyro, S. G., and Watson-Parris, D.: Aerosol absorption in global models from AeroCom phase III, Atmospheric Chemistry and Physics, 21, 15 929–15 947, https://doi.org/10.5194/acp-21-15929-2021, publisher: Copernicus GmbH, 2021.

Sander, R.: Compilation of Henry's law constants (version 4.0) for water as solvent, Atmospheric Chemistry and Physics, 15, 4399–4981, 2015.

Seinfeld, J. H. and Pandis, S. N.: Atmospheric Chemistry and Physics: From Air Pollution to Climate Change, Third Edition, John Wiley and Sons, 2016.

Skamarock, W. C., Klemp, J. B., Dudhia, J., Gill, D. O., Liu, Z., Berner, J., Wang, W., Powers, J. G., Duda, M. G., Barker, D. M., and Huang, X.-Y.: A Description of the Advanced Research WRF Version 4, Tech. Rep. NCAR/TN-556+STR, National Center for Atmospheric Research (NCAR), 2019.

Twomey, S.: The influence of pollution on the shortwave albedo of clouds, Journal of the Atmospheric Sciences, 34, 1149–1152, https://doi.org/https://doi.org/10.1175/1520-0469(1977)034<1149:TIOPOT>2.0.CO;2, 1977.

von Smoluchowski, M.: Versuch einer mathematischen Theorie der Koagulationskinetik kolloider Lösungen, Zeitschrift für Physikalische Chemie, 92, 129 – 168, https://doi.org/https://doi.org/10.1515/zpch-1918-9209, 1918.

Wexler, A. S. and Clegg, S. L.: Atmospheric aerosol models for systems including the ions H+, NH4+, Na+, SO42-, NO3-, Cl-, Br-, and H2O, Journal of Geophysical Research: Atmospheres, 107, ACH 14–1–ACH 14–14, https://doi.org/10.1029/2001JD000451, _eprint: https://agupubs.onlinelibrary.wiley.com/doi/pdf/10.1029/2001JD000451, 2002.

Zaveri, R. A., Easter, R. C., and Peters, L. K.: A computationally efficient Multicomponent Equilibrium Solver for Aerosols (MESA), Journal of Geophysical Research: Atmospheres, 110, https://doi.org/10.1029/2004JD005618, _eprint: https://agupubs.onlinelibrary.wiley.com/doi/pdf/10.1029/2004JD005618, 2005a.

https://doi.org/10.5194/egusphere-2026-2381
Preprint. Discussion started: 20 May 2026

Zaveri, R. A., Easter, R. C., and Wexler, A. S.: A new method for multicomponent activity coefficients of electrolytes in aqueous atmospheric aerosols, Journal of Geophysical Research: Atmospheres, 110, https://doi.org/https://doi.org/10.1029/2004JD004681, 2005b.

Zaveri, R. A., Easter, R. C., Fast, J. D., and Peters, L. K.: Model for Simulating Aerosol Interactions and Chemistry (MOSAIC), Journal of Geophysical Research: Atmospheres, 113, https://doi.org/https://doi.org/10.1029/2007JD008782, 2008.

Zaveri, R. A., Easter, R. C., Singh, B., Wang, H., Lu, Z., Tilmes, S., Emmons, L. K., Vitt, F., Zhang, R., Liu, X., Ghan, S. J., and Rasch, P. J.: Development and Evaluation of Chemistry-Aerosol-Climate Model CAM5-Chem-MAM7-MOSAIC: Global Atmospheric Distribution and Radiative Effects of Nitrate Aerosol, Journal of Advances in Modeling Earth Systems, 13, e2020MS002 346, https://doi.org/10.1029/2020MS002346, 2021.

Zhang, Y., Seigneur, C., Seinfeld, J. H., Jacobson, M. Z., and Binkowski, F. S.: Simulation of Aerosol Dynamics: A Comparative Review of Algorithms Used in Air Quality Models, Aerosol Science and Technology, 31, 487–514, https://doi.org/10.1080/027868299304039, 1999.

Zhang, Y., Seigneur, C., Seinfeld, J. H., Jacobson, M., Clegg, S. L., and Binkowski, F. S.: A comparative review of inorganic aerosol thermodynamic equilibrium modules: similarities, differences, and their likely causes, Atmospheric Environment, 2000.

Zhao, C., Liu, X., Leung, L. R., Johnson, B., McFarlane, S. A., Gustafson, W. I. J., Fast, J. D., and Easter, R.: The spatial distribution of mineral dust and its shortwave radiative forcing over North Africa: modeling sensitivities to dust emissions and aerosol size treatments, Atmospheric Chemistry and Physics, 10, 8821–8838, https://doi.org/10.5194/acp-10-8821-2010, publisher: Copernicus GmbH, 2010.

Zhou, P., Ganzeveld, L., Rannik, Ü., Zhou, L., gierens, R., Taipale, D., Mammarella, I., and Boy, M.: Simulating ozone dry deposition at a boreal forest with a multi-layer canopy deposition model, Atmospheric Chemistry and Physics, 17, 1361–1379, https://doi.org/10.5194/acp-17-1361-2017, 2017a.

Zhou, P., Ganzeveld, L., Taipale, D., Rannik, Ü., rantala, P., Rissanen, M. P., Chen, D., and Boy, M.: Boreal forest BVOC exchange: emissions versus in-canopy sinks, Atmospheric Chemistry and Physics, 17, 14 309–14 332, https://doi.org/10.5194/acp-17-14309-2017, 2017b.

Zhou, P., Cui, Z., Clusius, P., Makkonen, R., Fu, Z., Kerminen, V.-M., Kulmala, M., and Boy, M.: BoxMART - Box Model for Atmospheric Research and Teaching, https://doi.org/10.5281/zenodo.19591194, 2026.